February 2005 • NREL/SR-520-37659

Subcontractor Report

Productivity Enhancement for Manufacturing of Amorphous Silicon PV Modules

Final Technical Progress Report
1 July 2002–31 October 2004

H. Volltrauer and K. Jansen
Energy Photovoltaics, Inc.
Lawrenceville, New Jersey

National Renewable Energy Laboratory
1617 Cole Boulevard, Golden, Colorado 80401-3393
303-275-3000 • www.nrel.gov

Operated for the U.S. Department of Energy
Office of Energy Efficiency and Renewable Energy
by Midwest Research Institute • Battelle

Contract No. DE-AC36-99-GO10337

February 2005 • NREL/SR-520-37659

Productivity Enhancement for Manufacturing of Amorphous Silicon PV Modules

Final Technical Progress Report
1 July 2002–31 October 2004

H. Volltrauer and K. Jansen
Energy Photovoltaics, Inc.
Lawrenceville, New Jersey

NREL Technical Monitor: R. Mitchell

Prepared under Subcontract No. ZDO-2-30628-14

National Renewable Energy Laboratory
1617 Cole Boulevard, Golden, Colorado 80401-3393
303-275-3000 • www.nrel.gov

Operated for the U.S. Department of Energy
Office of Energy Efficiency and Renewable Energy
by Midwest Research Institute • Battelle

Contract No. DE-AC36-99-GO10337

Table of Contents

Table of Figures

Tables

PREFACE

This Final Technical Progress Report covers work performed at Energy Photovoltaics, Inc. (EPV) under PVMT&D contract, Prime Contract No. DE-AC36-99-GO10337, Subcontract No. ZDO-2-30628-14, titled PRODUCTIVITY ENHANCEMENT FOR MANUFACTURING OF AMORPHOUS SILICON PV MODULES.

EPV Contributors to the work are:

David Jackson
Barry Johnson
Joe Stallone
Steve Kane
Zoltan Kiss
Robert Lyndall
Krystyna Szewcsyk
Glenn Zitzer
Hermann Volltrauer
Robert McCort
Anthony Varvar
Kai Jansen
Leon Chen
Yuan-Min Li
Alva Sizemore
Bogulawa Wierzbowicz
Alan Delahoy

SUMMARY

EPV conducted parallel research efforts for achieving higher stabilized module power output through improvements in several manufacturing processing steps, with particular emphasis on the thin-film deposition process. The dual goals of achieving a 20% gain in stabilized output, and a 20% reduction in direct costs were accomplished.

The 20% gain in stabilized output increased the power of the standard 0.79 m^2 module to approximately 45 watts. This was achieved through optimizing the a-Si deposition process to improve stability, increasing the active area of the module, and by developing a ZnO/Al back reflector to increase the light absorption of the a-Si. Additionally, improvements were made to the a-Si uniformity, and an improved TCO was incorporated into the standard product.

The goal of reducing costs by 20% was exceeded, resulting in an estimated direct cost of $1.41/W, for the process in EPV's New Jersey facility. This was accomplished through a complete review of the process that resulted in lower material costs, lower labor costs, less downtime, and higher module power, as noted above. The process was streamlined and made more efficient by eliminating or combining process steps, and selected processes were automated.

In addition, improvements were made to the characterization and measurement techniques used in the module optimization process.

OBJECTIVE

The overall objective of this subcontract over its two-year duration is to continue the advancement of EPV's a-Si production manufacturing technology and improve the production equipment used in manufacturing. This will allow EPV to reduce module costs by increasing module output, throughput, and yield.

TASK 1 and 3: PRODUCTIVITY IMPROVEMENT

The objective of Tasks 1 and 3 were to 1.) combine or eliminate process steps, 2.) add automation, 3.) increase the throughput of the deposition system by 20%, and 4.) reduce both labor and material costs.

Overall Cost Reduction

M-1.4.6 - Demonstrate 20% Decrease in $/Watt for a-Si Modules from the EPV Production Line

Significant cost reductions were realized in both labor and material costs. The contributors to the reductions were: higher module output, elimination of shuntbusting as a separate operation, elimination of masking during sandblasting, reduction of deposition cycle time, and lower cost EVA, tin oxide and backing glass. Details of the reduction obtained in each of these areas are covered in their respective sections of this report, which immediately follow. In summary the cost reductions from these contributions are as shown in Table 1.

Table 1: Cost Reductions Achieved During this Program

	Material ($/Module)		**Labor (min. per module)**	
Process Step	**Before**	**After**	**Before**	**After**
Glass preparation	19.93	15.83	5.8	5.8
Laser TCO			7.5	4.9
A-Si deposition	1.97	1.97	8.7	7.2
Laser a-Si			4.8	2.9
Sputter back reflector	0.02	3.26	7.1	12.9
Laser back reflector			4.7	2.8
Shuntbust			2.4	0.0
Edge delete			11.9	6.0
Measure			1.8	0.0
Heatage			1.9	0.0
Measure			1.8	1.8
Encapsulate	14.12	11.96	27.7	27.7
Measure, clean, pack			7.5	7.5
Totals	**36.05**	**33.02**	**93.4**	**79.6**

Material costs are obtained from purchase orders and the application of an 85% yield for the thin film part of the process and 90% for the encapsulation. Labor costs are the durations, in minutes, of the individual process steps. The same yields are applied to the labor as for the material costs.

The cost of a module is based on a nominal labor cost of $20/hour wage with the additional assumption that for an eight-hour day, a worker will provide seven hours of productive work. As is discussed below, an output increase of 20% was achieved as a result of this program, which increased the stabilized power of the standard module from 37 W to 45W. The net result is a cost reduction from $1.94/W to $1.41/W as a result of this program, a decrease of approximately 25%.

Cost Reduction - Material

M-1.4.1 - Introduce Thinner and/or Lower Cost EVA onto the EPV Production Line

EPV has investigated two areas in which direct material cost reductions can be realized; less expensive EVA and a less expensive adhesive for the boot and bracket adhesion. Because EPV decided not to use the less expensive adhesive, it will not be discussed.

EVA - The cost of the EVA in the thickness range of interest, 12-18 mils, is nearly proportional to its thickness. Since the standard process uses an 18-mil product, the change to 12-mil thick EVA results in cost saving of approximately 30%. No difficulties were expected in using the thinner material and none were encountered. In the initial tests, about twenty modules were made with the 12-mil material. No lamination problems were discovered with these modules either in the lamination process or with the finished modules.

Prior to making these modules, a problem of excessive bubble formation around the perimeter of the modules, using 18-mil EVA, needed to be solved. Later in the program during routine encapsulation, a serious delamination problem came up, apparently resulting from incompletely cured EVA. Both were corrected.

In dealing with the delamination problem, a semi-qualitative test was developed for determining the degree of EVA cure by a non-chemical means. The procedure is based on an STR (Specialized Technology Resources, Inc.) "go/no-go" test and involves hanging a small weight from a narrow strip of the EVA to be tested while it is exposed to 80-90°C in ambient air. The EVA passes the test if, after 10 minutes, the strip has not elongated significantly, e.g. more than 10%. The test was made more quantitative by precisely controlling test conditions, and by making continuous measurements during the test. EVA samples were made by placing an eight by eight inch sheet of EVA on top of a sheet of 1/32" thick Teflon. Another thin sheet of Teflon was then placed over the EVA and the sandwich preheated for the standard amount of time. It was then placed in the laminator and covered with a piece of glass and laminated using a range of press times between 70 seconds and 310 seconds.

Figure 1 shows the result of the stretch test for six samples and Table 2 gives the gel-content measured by STR. The graph shows why this is a go/no-go test. The dividing line between the sample stretching quickly and hardly at all is a relatively small 10% range in cure times.

To obtain a quantitative measure of the extent of EVA cure, samples were prepared for gel-content determination. These tests were carried out by STR with whom we have cooperated on their PV Manufacturing R&D contract.

Gel-content determinations for some of these samples are given in Table 2. The numbers 12 and 18 under press time refer to the thickness of EVA. Both the gel-content and the stretch test suggest that the 12-mil EVA was not cured, yet modules made with the material appeared to be well bonded and show no signs of insufficient cure – contrary to the delamination discovered earlier with the 18-mil material. It is believed that the 5% gel-content measurement is an error.

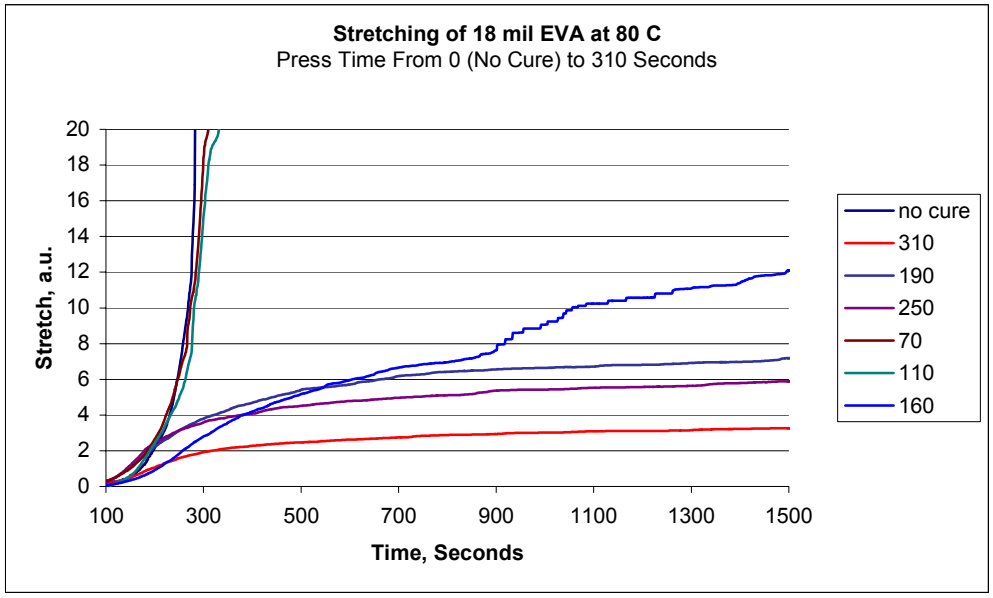

Figure 1: Effect of Lamination Press Time on EVA Cure

Table 2: Lamination Press Time and Gel-Content

Press Time, sec	Gel-Content, %
18 – 70	48
18 – 110	42
18 – 160	67
18- 190	77
18- 250	83
12 – 70	5

M-2.1.1 Identify Source for Lower Cost Tin Oxide

Testing of various types of tin-oxide is fully described in a later section (M-1.3.2). Over the course of this task, an improved tin oxide was identified, and a 23% reduction in its cost was negotiated with the supplier.

M-2.2.3 Complete Testing and Analysis of the use of Thinner Backing Glass in EPV a-Si Modules.

The main advantage of using thinner backing glass in modules is a product with lighter weight and lower cost. The approximately 16% thinner backing glass has reduced the module weight by about 8%, and the cost savings for the glass is about 28%. With the backing glass being close to 10% of the material cost, the thinner glass lowers that cost by almost 3%.

The major concern regarding the use of thinner backing glass is its strength. To evaluate the strength of both the standard product and the new thinner backing glass module, a series of static load and bending tests were initiated. Laminated and non-laminated glass coupons were compared as well as full sized laminated modules to understand the key parameters affecting glass strength, including glass edge treatment and glass thickness.

The strength testing was begun on standard non-laminated 3.3 mm glass test coupons. For these initial tests, the standard clear back glass was evaluated using a standard three-point load test. This involved supporting a glass sample on two ends and applying a weight to the center of the test sample as shown in Figure 2. For these tests, a seamed piece of glass was used that was 8" x 49" instead of the standard 25" x 49" full-sized sheet. This allowed the rupture stress of glass to be reached at a lower applied weight, and thus helped to accelerate the testing. The glass was cut and seamed using the standard production line processes.

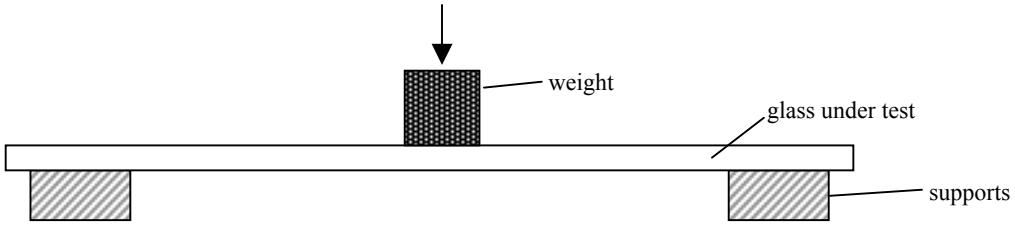

Figure 2: Three Point Static Load Test

The baseline strength of the standard glass was determined by continuously increasing the weight until breakage occurred. For the 8" x 49" seamed glass sample, the breakage typically occurred at approximately 6 lbs applied weight, not including the weight of the glass. This agreed reasonably well with the predicted breakage for 3.3 mm weathered annealed clear glass, which can be calculated using the formula for the modulus of rupture for a three point simply supported beam [1]:

$S = 3PL / (2bd^2)$

Where:

S = modulus of rupture (psi), 6000 psi for weathered annealed glass (for a 60 second load test)
P = force required to break the glass (lb)
L = unsupported span (in), (49"minus two 2" supports = 45")
b = width of sample (in), 8" for these tests
d = thickness of sample (in), 0.125"

Rearranging this formula and solving for the force required to break the glass, P, the predicted force to break the glass within 60 seconds, is calculated to be about 11 lbs.

Since the glass in these test weighs ~ 4.25 lbs, the total weight causing the breakage is ~ 4.25 lb plus 6 lb or about 10 lbs, with the understanding that the weight of the glass is uniformly distributed over the length of the sample and is not concentrated at the center, and thus results in a correspondingly lower stress than its mass would otherwise indicate. The agreement with the predicted breakage force is nonetheless fairly good, and this type of test has been used to

optimize the edge seaming process in another research program. As a result of that program, the breakage strength in similar tests has increased by approximately 75%, by changing to a finer grit belt in the seaming operation.

To understand the effect that glass thickness had on laminates, a deflection/breakage test was carried out on laminate coupons. The graph shown in Figure 3 shows the deflection and ultimate breaking strength of three types of 48" by 2" laminate structures using single strength (2.5 mm) and/or double strength (3.3 mm) glass. The three laminates are single/single (s/s), single/double (s/d) and double/double (d/d). The graph is an example of the behavior of three laminates as a slowly increasing force is applied to the center of the test sample. All three samples were seamed as described above and tested until failure.

As can be seen in the figure, there is approximately a 25% reduction in breakage strength with a s/d laminate when compared to a d/d laminate in this test. As expected, the s/s laminate has even lower breakage strength at approximately 60% of the d/d configuration.

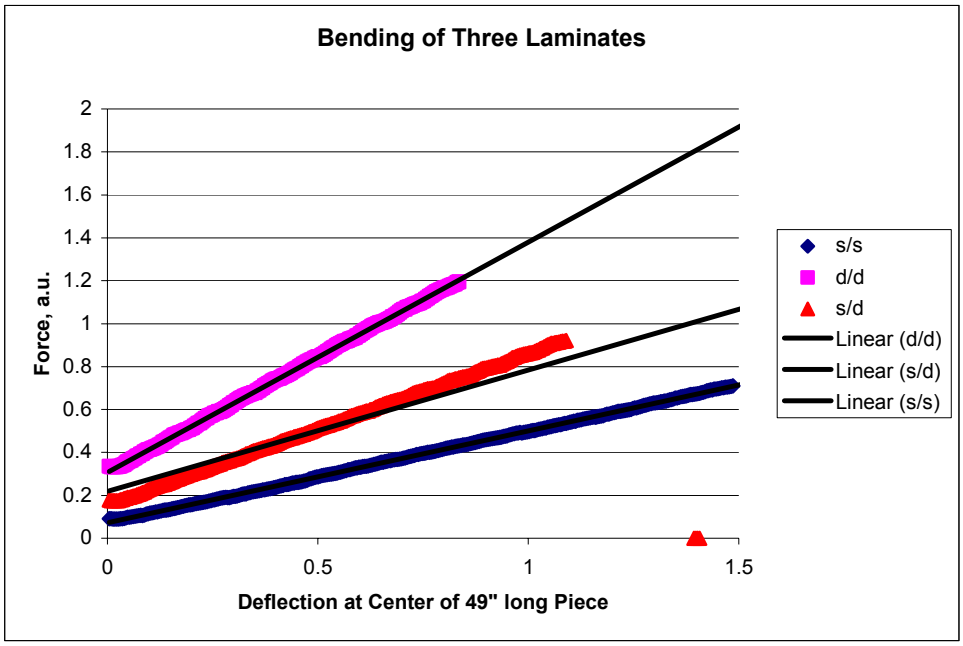

Figure 3: Deflection of Three Laminates Under Load

The evaluation of the thinner backing glass was completed by preparing full sized modules and subjecting them to static load testing. The modules were loaded uniformly with sand bags to the standard test weight of 50 lb/sq.ft., which they passed without breaking. To determine the safety margin, the tests was continued to destruction, which occurred at approximately 72 lbs/sq.ft., well in excess of the 50 lbs/sq.ft. load of the standard test.

Cost Reduction - Labor

The labor required to manufacture a plate was reduced by nearly 15%, as summarized in Table 1. This labor reduction was the result of streamlining the process, reducing a-Si cycle time, improving the equipment, and by selectively automating key process steps as described below.

M-1.1.2 Eliminate Need for Masking Plates During Edge Film Removal

As demonstrated in many reliability tests, the sandblast method of edge delete is the preferred process throughout the industry to ensure electrical isolation of the encapsulated module. This process was adopted years ago by EPV because it was less expensive and more consistent than the previously used laser ablation process. It created a wide edge delete very quickly and gave the module an attractive "framed" appearance.

In EPV's original process, masking of the plate prior to sandblasting was needed because the sandblasting process generated dust and debris that was difficult to remove from the plate and the damage from the sandblasting extended over a relatively large region. A benefit of the masking was that the edge of the sandblast region was well defined, however the downside was that it was a very labor-intensive, manual procedure. To eliminate masking, the sandblasting process had to be improved, both to better define the region sandblasted and to make it a cleaner process. These objectives were met with a new prototype single-head sandblaster. By changing the vacuum pickup system, debris was efficiently removed. In addition, a static discharge system was added to the machine to prevent blasted debris from gravitating to the surface of the glass. Precisely directed air jets in the blasting area helped direct the debris into the pickup and also resulted in the required sharp dividing line between the sandblasted region and the film.

To determine how well defined the sandblasting boundary was, the distance from the sandblast edge beyond which there is no damage was determined. This was done with a specially prepared small plate in which the aluminum film adjacent to the sandblast edge was removed in steps by sputtering with a mask, and the shunt resistance of the resulting cells was measured. The results of such a test are shown in Figure 4. Shunt resistance was measured between two adjacent cells and the distance was measured from the edge of the plate to the beginning of the aluminum film. Shunt resistances higher than full scale at 200 ohms were recorded as 200 ohms. The sandblasting removed 0.375 inches of thin films around the perimeter of the plate, and Figure 4 shows that significant damage stops shortly after 0.375 inch. Since the cells on the standard plate do not extend to within about 0.625 inches from the edges of the plate, the improved sandblasting head does not cause any damage to the module.

In addition to providing a sharply defined sandblast area, the modules also easily passed the leakage test at 2.5 times the system voltage plus 1,000V (i.e. 2,500VDC).

The cost savings resulting from avoiding the masking and combining the laser isolation step with the initial tin oxide lasering, amounts to an approximately 6% reduction in direct labor costs. This reduction is the combined time of masking the plate with paper, removing the paper, cleaning, and transporting the plate to the stations involved.

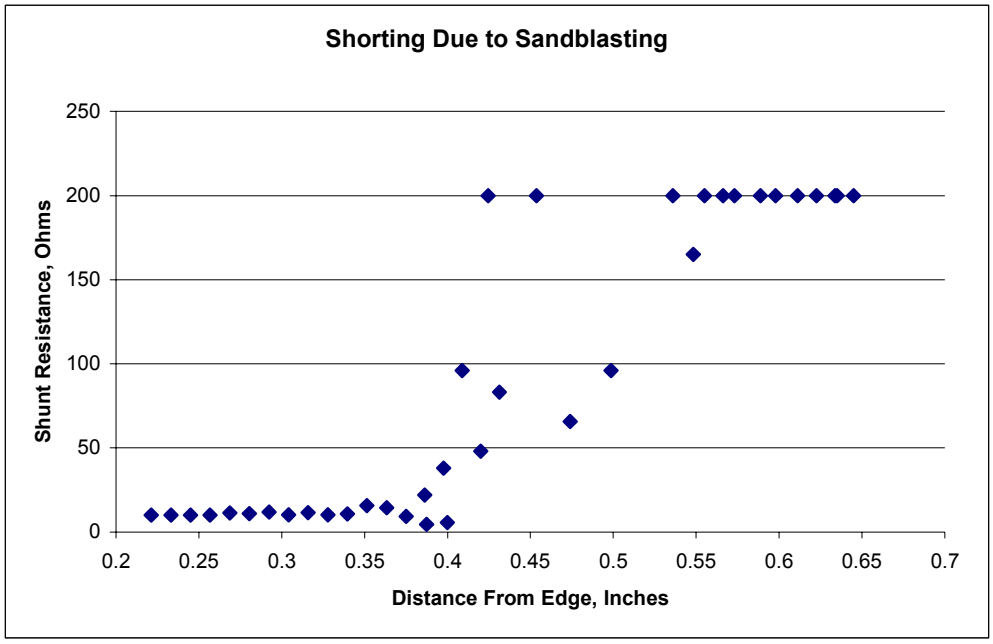

Figure 4: Damage Caused by Sandblasting

M-1.2.1 - Complete a 20% Reduction in the a-Si Deposition Cycle Time for Tandem Devices.

At the start of this program, the a-Si cycle time for tandem runs was approximately 4.8 hours. The steps immediately before and after this step, the pre-heat and cool-down, had process times that were shorter than this, and therefore a reduction in the a-Si cycle time had the potential to increase throughput. Of the 4.8 hour cycle time for a deposition run, about 3.5 hours were used for pumping down the system, mostly in the hi-vac mode. To determine the effect of shorter deposition cycles, six runs were made with variations to this pump-down sequence. Two hi-vac pumping sequences were targeted for reduction 1.) the initial pump down from atmospheric pressure and 2.) the pump downs between the p and i-layers. Each of these was replaced with a period of rough pumping followed by backfilling the chamber with hydrogen, and then quickly pumping the chamber to an intermediate pressure.

Both single and tandem junction runs were made with the modified pump down sequence. With the deposition times being the same for the comparisons, the total times from door closing to venting were as follows:

	Standard Process	Reduced Cycle Time
Single Junction	3.4 hours	2.5 hours
Tandem Junction	4.8 hours	3.6 hours

In both cases the cycle time reduction amounted to approximately 25%. The initial power output from the reduced cycle time plates was essentially the same as the power output from plates made in deposition runs using the standard process. To minimize scatter arising from run to run variations and to make it easier to detect small changes in performance between these process changes, several pumping variations were tested in different RF sections of a

single a-Si batch. In this deposition run, two variations of the initial pump down sequence were tested along with three variations of the pump down between the p and i-layers. A single junction run was chosen, because compared to a tandem run, there are fewer pump downs and the degradation is greater than for tandems, making module stability differences easier to detect.

In this run, a shorter 20-minute pumping sequence was used for the initial pump down, compared to the standard 50 minutes, and the p-layers were deposited on twelve plates in three RF sections. Next, the system was pumped down using the standard 50-minute procedure, and p-layers were deposited in three additional sections. Three pumping variations were then used between the p and i-layers. First, a short pump down was completed and an i-layer was deposited on one section of the short and one section of the standard initial pump down thereby replacing the 50-minute process with a 20-minute process. Next, a second 20-minute pump down was completed and an i-layer was deposited on a second of each of the two initial pump downs. The system was then pumped with the standard 50-minute pump downs and i-layers were deposited on the two remaining sections.

Averaged initial results for the six variations of this run are shown in Table 3.

Table 3: IV Parameters Before Light Soaking for Reduced Cycle Time Deposition

RF Section	initial min	p to i min	Voc V	Isc A	FF %	P W
4	20	20	59.2	1.059	70.1	43.9
5	20	40	59.6	1.068	68.0	43.3
6	20	50	59.6	1.083	67.7	43.7
7	50	20	59.4	1.084	67.7	43.6
8	50	40	59.2	1.082	68.6	43.9
9	50	50	58.8	1.083	68.6	43.7

Within the precision of the measurements, the parameters for all six variations are essentially the same. The only possible trend pertains to the three short initial pump downs, in which Isc increases and FF decreases as the "p to i" pump down time is increased. This "trend" is very likely due to measurement uncertainty, since the opposite is expected, at least for FF.

To determine the stability of the plates, two light soaking studies were done: accelerated light soaking (ALS) and outdoor exposure. The same plates were used for both studies. One plate from each of the six pump down variations was cut into three sections: one 3-inch wide section from the center, and the two 23-inch wide sections from the two sides. The two larger plates were made into "half-modules" and a 3x3 inch piece was cut from the center section on which small, isolated devices (dots) were made. The "half-modules" were light soaked outside, while the dots were subjected to ALS at approximately 47 suns for 162 seconds. While ALS does not predict the module's stabilized performance, it can reveal differences in stability between different devices (see details under Measurements at the end of this report).

Table 4 compares the electrical parameters for the six cut plates subjected to ALS at 0 and 162 second, as well as their percentage changes.

Table 4: Effect of ALS on Reduced Cycle Time Deposition

Pump Down		Voc,mV			Isc, mA			FF, %			Eff, %		
initial	p to i	at time , sec.		change	at time , sec.		change	at time , sec.		change	at time , sec.		change
min	min	0	162	%	0	162	%	0	162	%	0	162	%
20	20	778	802	3.1	12.3	11.2	-8.8	72.7	55.5	-23.7	6.93	4.97	-28.3
20	40	779	805	3.3	12.2	11.1	-8.9	71.6	55.5	-22.6	6.81	4.96	-27.1
20	50	784	806	2.8	12.7	11.3	-11.5	70.3	54.1	-23.0	7.02	4.92	-29.9
50	20	779	804	3.2	12.7	11.3	-11.3	70.1	53.9	-23.2	6.96	4.90	-29.6
50	40	779	798	2.5	12.6	11.2	-10.6	71.3	53.9	-24.4	6.99	4.84	-30.8
50	50	778	798	2.5	12.6	11.4	-9.3	72.4	55.3	-23.7	7.09	5.03	-29.0

No real trends are apparent. For the half modules light soaked outside, the following was obtained.

Table 5: Effect of Outdoor Light Soaking on Reduced Cycle Time Deposition

Pump Down		Voc, V			Isc, A			FF, %			Power, W		
initial	p to i	at time , days		change	at time , days		change	at time , days		change	at time , days		change
min	min	0	35	%	0	35	%	0	35	%	0	35	%
20	20	58.9	61.4	4.3	483	419	-13.3	69.2	57.5	-17.0	19.7	14.8	-25.0
20	40	59.0	60.9	3.3	482	408	-15.4	65.2	59.2	-9.2	18.5	14.7	-20.7
20	50	59.8	61.8	3.3	494	439	-11.3	66.0	57.6	-12.7	19.5	15.6	-20.0
50	20	59.5	61.4	3.2	492	433	-11.9	66.4	56.7	-14.5	19.4	15.1	-22.3
50	40	59.2	61.1	3.3	495	433	-12.4	67.4	57.1	-15.2	19.7	15.1	-23.3
50	50	59.0	60.6	2.7	495	437	-11.5	68.3	57.9	-15.1	19.9	15.3	-22.9

As is the case with ALS, no real trends are apparent. Based on this information, it can be concluded that the shortened pump-down used in these runs do not have a deleterious effect on module performance and a 20% cycle time reduction has been achieved.

M-1.3.1 - Reduce Labor Costs by Eliminating or Combining Process Steps

Two process steps were eliminated or folded into other steps, heat-aging and shuntbusting. An argument can be made that the former can be done on a sampling basis rather than for all plates, and the latter can be made part of the IV test procedure where it requires no additional labor to carry out.

A. Heat-Aging

The standard process at the start of this program included a heat-aging step in which the plates were brought to 150° C and held for one hour. This step served two purposes. First, it was a quality control (QC) test that was intended to verify that the internal tin oxide to aluminum contacts were good, and second, it typically resulted in a few percent increase in power output of the plate.

QC - The QC function of the heat-aging step relies on heat stressing poor contacts, mainly aluminum to tin oxide, but also aluminum to a-Si, in order to make them worse and therefore easier to detect. Poor contacts also result in poor adhesion of the aluminum and can usually be detected in the "peel" test that is carried out after sputtering of the aluminum, by applying,

then rapidly pulling off a 2" strip of tape. Over the course of this program, several runs with heat-age failures were experienced, defined as a drop in FF of more than 5%, but in these cases the plates affected also failed the "peel" test.

Power Gain - It is likely that heat-aging produces no long-term power gain. It is known from past experience that the gain resulting from heat-aging can be obtained at different temperatures. Figure 5 shows actual conditions previously used by EPV personnel for heat-aging a-Si plates. A fit of the temperatures to log (time) results in a surprisingly straight line. The temperatures and times initially chosen for these tests were based on QC considerations, but all of them also resulted in power gains of the plates.

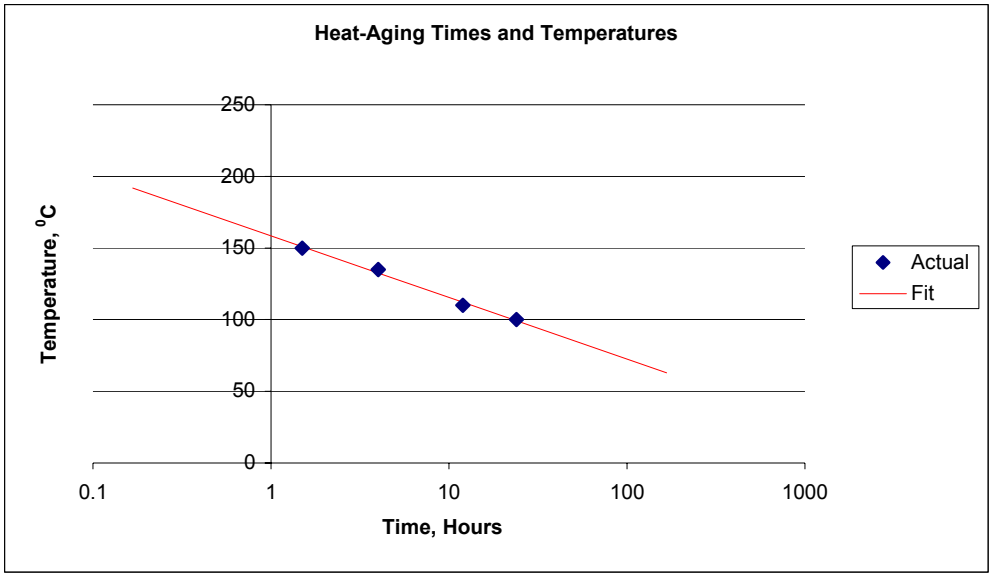

Figure 5: Relationship Between Temperature and Heat-Age Time

If the extrapolations were to be valid, then at 55°C, corresponding to the approximate module temperature in full sunlight at 20°C ambient, less than two weeks would be needed to realize the "same" effect as 1.5 hours at 150°C. While this has not been experimentally verified, it seems likely, and since it takes an a-Si module several months to stabilize it may well be sufficient to realize the full heat-age gains. The net result of not heat-aging in the manufacturing process is expected to be a smaller initial Staebler-Wronski degradation than if they had been heat-aged. Since the heat-age gain is typically 3-5%, the degradation will probably be reduced by that amount.

Cost Saving - Labor cost savings from eliminating heat-aging or combining it with the lamination process can be determined in the ideal case in which there are no heat-age losses. The current heat-age process including transferring the plates to the oven, as well as loading and unloading the rack takes approximately 1.5 minutes per plate. An additional 2 minutes is taken up by a measurement step. Eliminating both will result in a labor savings of 3.5 minutes or 4.4 %.

Based on the above considerations, heat aging has been discontinued and is only carried out for special testing.

B. Shuntbusting Process

Lasering of the aluminum back contact separates the individual cells, but leaves some cells with residual electrical shorts in the range of a few tens to a few thousand ohms. Some of this shunting is the result of incomplete separation (see also M-1.2.2). Reverse biasing or shuntbusting the shorted cell at 4-5V, usually removes most of these shunts. In the original process, shuntbusting was done at three locations of every cell of every plate; a time consuming operation.

It has been determined that very similar results can be obtained by treating the entire PV plate or module at one time. This is done by discharging a small, 270-microfarad capacitor, charged to approximately 150 V, through the plate in the forward direction. This procedure also eliminates most shorts and typically gains an additional 1-2% of the measured power when applied to a finished module that had already been shuntbusted cell-by-cell. The procedure works well for tandem modules, but is not very effective when applied to single junction modules because the voltage developed across each cell is only about 2 V, with the capacitor charged to 150 V.

To evaluate this procedure, several tests were carried out in which the plates are first shuntbusted as full plates and then cell-by-cell. For three such tests, the average changes in electrical parameters resulting from the full-plate shuntbusting and subsequent cell-by-cell procedure are given in Table 6.

Table 6: Full Plate and Cell-by-Cell Shuntbusting

	Voc	**Isc**	**FF**	**P**
Change after full-plate shuntbusting (%)	2.1	-0.3	3.5	5.3
Change after additional cell-by-cell (%)	0.1	-0.1	1.3	1.2

The reverse order was also carried out, following the cell-by-cell shuntbusting of 23 plates by full plate shuntbusting. This second procedure resulted in a 2.5% additional gain in power output. Two to three percent is also the typical gain obtained when completed modules, which had been routinely cell-by-cell shuntbusted, were subjected to full plate shuntbusting procedure during their final IV test prior to packing. Based on these data, the full plate shuntbusting appears to be a viable alternative to the time consuming cell-by-cell process and is now part of the process.

Cost Savings - The process of carrying out the cell-by-cell shuntbusting takes approximately 2.4 minutes per plate. EPV's total labor content per module is approximately 93 minutes, making the labor saving 2.6%.

M-1.4.2 – Complete Upgrade of the RF Matching Network on One Section of the EPV Production Line from Manual to Automatic

The development of the automatic matching networks was carried out in stages. First, the current manual matching networks were characterized and the range of capacitances needed for the discharges involved were determined. The effect of small mismatches was then determined and prototype matching networks were built and tested. The final versions of the matching networks were then assembled, installed, and qualified.

During the development phase, three approaches were tried. The simplest approach was to only preset the tuning capacitors and tolerate some amount of reflected power. Secondly, a new circuit design was evaluated, first as a manual network and then with automation added. Lastly, it was decided that the current units did a very good job and proceeded to add the necessary components to them to automate them.

A. Characterizing the Existing Manual Networks

In the first test, the reflected power was measured while first the input, and then the output capacitors were changed to detune the circuit; in each case the other capacitor remained fixed. As Figure 6 shows, the input capacitor has relatively little effect on reflected power; the capacitor readings are the deviations from their original tuned point.

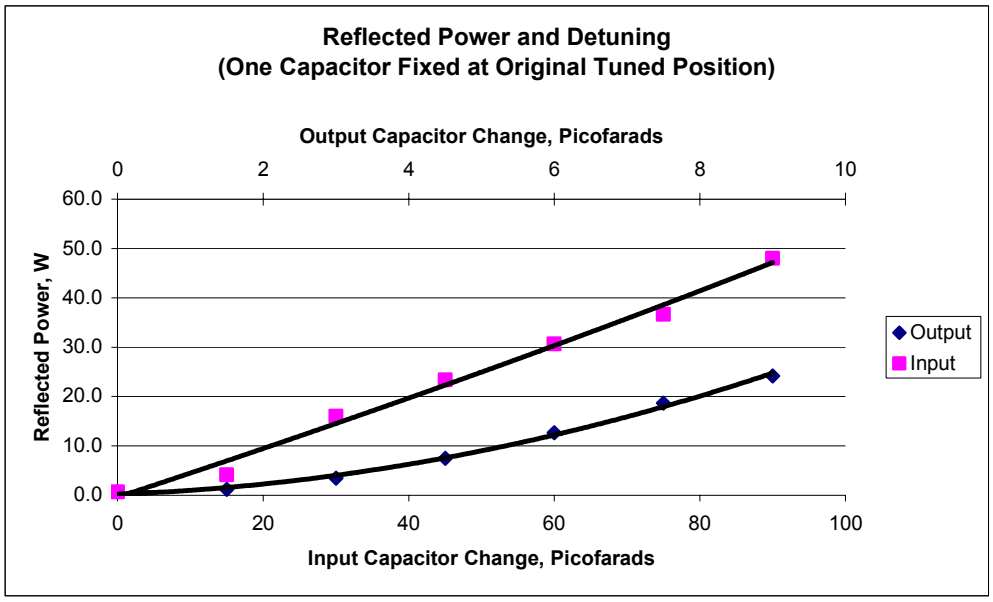

Figure 6: Reflected Power and Detuning

The effect of deposition system pressure changes was also investigated and found to be small.

Restarting the discharge ten times and tuning for minimum reflected power checked repeatability. As seen in Figure 7, the output capacitor is within a range of approximately 5 picofarads for the ten tests which, from the graph above, corresponds to about 30 W reflected power.

To determine if reflected power levels of the magnitudes observed above have any effect on the quality of the plates made under such a condition, a run was made in which two sections were deliberately detuned to achieve a reflected power of approximately 30% of the input power to the matching network. In this test, the RF current delivered to the discharge was held constant. Averaged electrical parameters of the plates made with a 30% reflected power, and in the same run with essentially zero reflected power are summarized in Table 7.

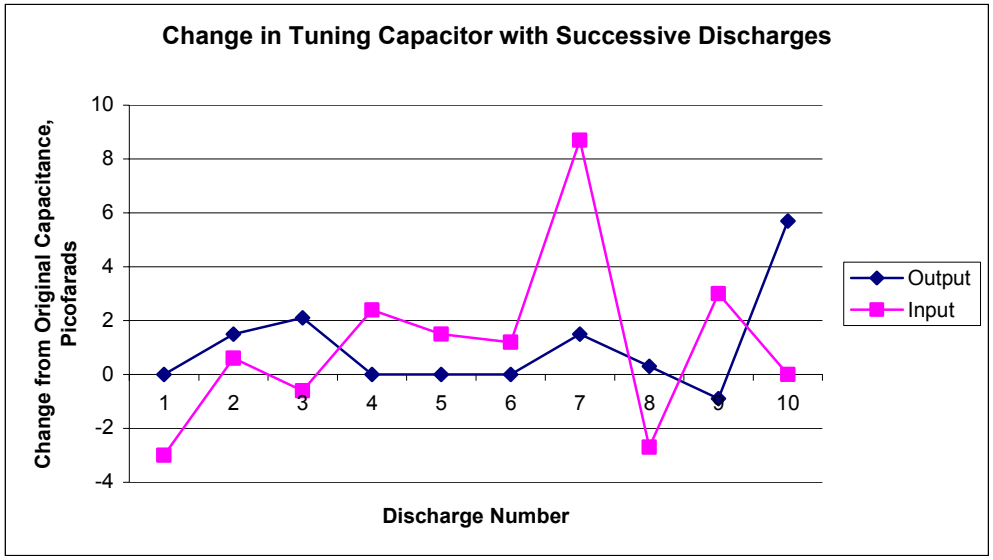

Figure 7: Change in Tuning Capacitor with Successive Discharges

Table 7: Comparison of IV Parameters for Depositions Made With and Without High Reflected RF Power

Reflected Power (%)	Voc (V)	Isc (A)	FF	P (W)
30	62.9	1.24	63.6	49.7
0	62.7	1.22	63.1	48.4

No significant difference between the plates was observed. Based on these results, a very simple "automated" matching network could be built that simply pre-selects the capacitor setting that brings it to the approximate point needed for low reflected power. By tolerating a relatively small amount of reflected power, a fine feedback-controlled tuning device is not required. A prototype matching network was built as suggested above, i.e. with only using preset values and it worked adequately.

B. Automated Network

While the preset-only network would probably suffice, it did not provide much information regarding the discharge. For this reason it was decided to build a more active network. First a directional coupler and appropriate electronic circuitry was added to the current network to measure RF voltages and DC bias. These additions are intended to allow the acquisition of more detailed information regarding the deposition conditions. For example, the DC bias measurement reveals whether the discharge is on or not and is used to trigger the start of tuning when plasma is present.

The directional coupler uses a printed circuit board as a 50 ohm stripline with 2 pickup loops to measure forward and reflected power at the input to the matching network. It is calibrated to match the automated matching circuits. The forward and reflected power signals are both available for further data analysis.

Small commercial stepper motors were added to drive the variable capacitors used to match the load. Smaller capacitors than in the manual networks were also selected so as to be able to fit all the components into the same space as used by the manual networks. This is important since twelve networks were needed for a system capable of processing forty-eight sheets of TCO glass, and the physical size of the twelve networks had to fit in the same space as the original networks.

Features of the automated networks are:

1. The use of 4 vacuum relays used with the 4 variable capacitors on the primary (tune) side of the tuner – this allows presetting the capacitance to the estimated final set point. While this worked well in the prototype unit, a stepper motor was added to the primary to allow better control especially when using multiple substrate carriers that may have different impedances.
2. The start of auto-tuning is now controlled by the DC bias signal, which is only present when there is plasma.
3. The tuners also contain software logic for an automatic "learn" mode. In this mode, the matching network remembers the capacitor settings for each layer and applies these settings for the next run.
4. Additional signals are made available to be monitored by the deposition system for analysis. These include RF voltage and current, DC bias voltage, forward and reflected power.
5. The tuner now contains an embedded micro controller that carries out the tuning in addition to a stepper motor, microstepping drive, and signal processing circuits. Various filters were added to minimize noise in the control circuits.
6. To make better use of the limited space available in the enclosure, the power supplies used for the local electronics are located externally.

This tuner has been in use for several months and has worked very well.

M-2.4.1 – Automated Remaining RF Matching Networks.

As a result of using automated matching networks in all twelve RF sections, labor costs have decreased, the deposition process has become more reliable and repeatable, and there is access to additional process information that was not previously available.

The installation and optimization of all twelve matching networks proceeded as expected. After initial fine-tuning of the system, all networks repeatably ignited the plasma and correctly minimized the reflected power for each RF section. The first matching network has been in use for several months and it has required no operator attention whatsoever.

The automated matching networks contain the following sub-components:

Directional coupler
DC bias detection circuit
Analog processing circuits
Microcontroller with EEPROM data storage
Stepper motor driver circuits

Adjustable tuning components

Each of these was calibrated and functionally tested before being installed on the deposition system. Small test software programs were written for this purpose.

Once the matching networks were installed on the system they were individually powered and tested with a real plasma and with tin oxide coated glass. Initially Argon was used to fine-tune the software.

After reliable performance was obtained with Argon plasmas, the deposition mixtures were tested. First the networks were manually tuned to obtain the pre-tune positions for each layer. This information was then entered into the EEPROM of each matching network. Repeated real depositions were then carried out to verify performance.

The auto-tuners have an "auto-learn" feature that stores the tuning component's positions once each layer has been completed. These positions serve as the starting point for the next run. In case the auto tune should fail, the tuners have a manual adjust feature that would allow the operator to complete a run.

Operation thus far shows these tuners to perform better than the operator set manual tuners, not only in the speed of establishing tuned conditions, but in the fact that there is essentially no reflected power. When manually tuned, there would typically be a few sections with several percent reflected power. Several benefits of automating the matching networks have been realized including:

Labor savings - Tuning each manual network takes about 5 seconds per RF section. For the twelve sections doing tandems, that amounts to 72 tuning steps or six minutes. Since several people are used during the manual tuning process during the p-layers, and these people are pulled away from other tasks, the actual total time lost is on the order of 30 minutes. Factoring in yields and labor, the total direct labor savings is approximately 1%.

Reliable operation - Because it was shown that some modest degree of detuning is not detrimental to performance of the PV device, there is no gain in output arising from an improvement in a-Si material quality from the use of the automated networks. However, since the networks do not require operator intervention, the process is more repeatable and reliable. This is expected to increase process yield and result in an increase in productivity.

Information – The automated matching networks provide additional information that may be beneficial in process optimization and control. Long term it is expected that this additional information such as the DC bias signal (which is only present when there is plasma), RF voltage, RF current, and both forward and reflected power will provide some insight into the deposition process.

The full benefit of the automated matching networks may not be known for some time but the cost savings and reliability of the system currently obtained justifies its implementation.

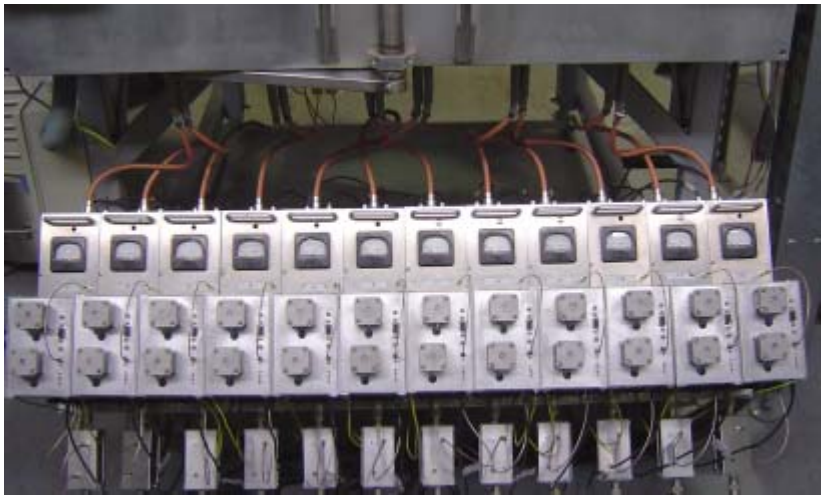

Figure 8: Photo of Twelve Automated Matching Networks

M-1.4.3 - Complete Study and Automation of at Least One Process Step

The current manufacturing process was reviewed and the cost and gains resulting from automating various steps has been estimated.

From this analysis two process steps were selected as candidates for automation and one was automated in Phase II. The selection was based on two major criteria, 1) reducing the direct labor component of that particular step, and 2) upgrading or replacing the equipment in that process step to improve the equipments reliability, performance, and throughput; and/or increase the quality of the equipment's output. In addition to these criteria, operator safety was not to be compromised. The two process steps initially identified were 1) automating the seamer and the seamer to washer transfer, and 2) the sputtering system unload; the latter was automated.

A. Seamer

With the seamer, the second criteria, improving equipment performance and quality of output, was the primary desired outcome. The currently used seaming operation uses a Prestik 2 belt wet seamer with two 4" X 106" 80 grit sanding belts and a 36" X 78" roller table. To seam a piece of glass the operator must rotate the glass substrate on the roller table while maintaining contact with the 2 belts. This process has been found to have an inherent repeatability problem both from the operator 'processing' side and from an equipment side as the sanding belts wear down. As edge defects are a primary cause of plate and module breakage as the substrates are stressed, the importance of producing a uniform, seamed edge cannot be minimized. The intention was to replace the current equipment with a heavy-duty single or multi-spindle automatic glass edger, such as the Somaca VE-1A. This, or a similar machine, has the capacity to produce various uniform and consistent edges like a pencil edge and/or a flat and seamed edge that is not operator or sanding belt dependant. There was also the possibility of increasing throughput and reducing labor costs by automating this process step.

B. Sputtering Unloader

Reducing labor costs, was the primary motivation for selecting this step. Automating this step would also resolve a potential employee safety issue.

The cost savings comes from better utilization of the operator's time. Although the sputtering process is fully automated, the operator must still be present to unload the substrate at the proper time to achieve the required throughput. Automating this step would reduce the operator's time constraints so that a high throughput can be more easily obtained. The fully automated unloading system 1) opens the exit chamber door, 2) transfers the glass to a buffer type storage area to await aluminum scribing, and then 3) closes the exit chamber door. This system also eliminates a potential safety issue as the current unload procedure requires the operator to remove the substrate from the exit chamber at an exit chamber height of nearly 60 inches.

M-2.3.2 - Automate One Process Step

Based on the rationale described above, the sputtering system unloader was selected for automation.

The automated unloader for the sputtering system was designed built, installed, tested and is currently in use on the production floor. The main components of the unloader, as shown in Figure 9, are the base and frame, a scissor jack, a transport stage and the control electronics. Two additions to the sputtering system were also made, the automatic exit door actuator and the entry and exit light stacks.

The support structure is made with 80/20 aluminum extrusions and supports the translation stage, transport drive, and control box. A safety bar has been added on the translation stage to stop the movement if an object is in its path. Leveling and height adjustments are also provided.

The translation stage contains a programmable logic controller (PLC) that was incorporated to reduce the amount of down time during installation. The system is now controlled by the sputtering system's own PLC; it is interfaced to the sputtering system's main control system by means of a serial connection. By communicating serially, the overall wiring has been reduced significantly and the system is a modular design.

An air cylinder is used to open and close the door. Its operation and the switching of entry and exit light stacks, which notify the operator of system status, have been programmed into the sputtering system's control logic.

The unloader has been operational for several months and is working well. While it reduces the cycle time by a modest 6 to 10%, the operator can use the nearly four minute window to:

1. Prepare the plates for sputtering more carefully.
2. QC for plates in and out of the sputter system.
3. Pay more attention to the overall operation of the system and record more process information.

Figure 9: Photo of Automatic Unloader on Sputtering System

Milestones Not Directly Related to Cost Reductions or Output Increases

Several tasks were completed that did not have a direct effect on performance improvement and cost reduction. These tasks included the comparison of manufacturing single junction vs. tandem modules, an analysis of downtime and the development of an automated run analysis program.

M-1.1.1 Complete Comparison of Benefits of Manufacturing Single Junction and Tandem a-Si Devices

The analysis of single junction and tandem modules was divided into manufacturing or cost related issues, and quality issues. A third point for analysis was the change in relative advantage of both types of modules that would result from improvements that are planned under this contract for the near future. These considerations are discussed below.

A. Manufacturing and Cost Related Issues

The complete a-Si deposition cycle time for single junction modules is approximately 70% of the tandem cycle time. A relative manufacturing cost savings will be realized when manufacturing single junction modules, because a shorter cycle time will result in reduced labor, electricity use, gas consumption, liquid nitrogen use, and gas scrubber costs.

In principle, less deposition equipment is required for single junction modules. For example, the EPV batch process for a 5 MW per year tandem junction facility requires two deposition systems. With a fairly modest reduction in deposition cycle time for single junctions, to slightly under 2.5 hours, only one deposition system with all the associated components is required for a 5 MW per year facility. This represents a considerable savings in equipment costs.

Lower laser costs for tandems partially offset their higher deposition system costs. About one-half of the number of laser scribes is required for a tandem module compared to a single junction module; therefore, tandem module manufacturing facilities require fewer lasers per scribe station which reduces equipment cost.

In full-plate shuntbusting (see M-1.3.1), shorts are cured (or "burned out") by discharging a capacitor through the plate as part of the IV Testing procedure. This full-plate shuntbusting is not as effective for single junction plates, since much higher currents must be passed to generate voltages similar to those developed on tandem plates; therefore, a separate shuntbust station would be required for single junction facilities.

Cost Comparison - The standard silicon deposition process for tandems required about 4.5-4.8 hours from door closing for one run to door closing for the next. For a tandem module facility with a 5 MW per year capacity, two complete deposition systems with pre-heat and cool-down chambers are required. Table 8 lists the time available per single junction deposition run using one deposition system for a 5 MW per year operation and taking into account the length of the workweek and yield.

Table 8: Deposition Cycle Time for Single Junction Operation

Operation	80% Overall Yield	90% Overall Yield
5 day/wk	1.84 hrs	2.07 hrs
6 day/wk	2.21 hrs	2.49 hrs

Based on several tests carried out during the past year (see M-1.2.1), the 2.49 hours is very likely achievable with a single deposition system when making single junction devices; even the 2.21 hours is within reach. In the cycle time reduction tests discussed under M-1.2.1 with tandems, the shortest deposition cycle time achieved was about 3.5 hours. Considerable cost savings can be realized when building a factory that makes single junction modules compared to tandems. Material and electricity costs are also impacted. The costs will be looked at from the point of view of changing to single junction modules from tandems.

Equipment – To increase the capacity of a 2.5 MW per year tandem operation to a 5 MW per year single junction operation, an extra laser and associated optics has to be added to the three laser stations, for a total of one IR and two green lasers. In addition, a shuntbust station is required. This upgrade would cost approximately 7% of the total equipment cost of the 2.5 MW per year tandem facility. To upgrade a tandem line from 2.5 MW per year to 5 MW per year, a second deposition system is required. This upgrade would cost approximately 20% of the equipment cost of the 2.5 MW per year tandem facility. An approximately net 13% equipment cost saving can be realized when increasing the capacity of a 2.5 MW per year tandem operation to a 5 MW single junction process compared to a tandem process.

Material - Depositions for single junctions will be slightly shorter, mainly due to shorter gas stabilization times. Less gas, fewer scrubber cartridges, and less liquid nitrogen will be used, for a total saving of approximately 4% in material costs. The LED arrays for the lasers will be used less with tandems and thus increase material costs for single junction by approximately 1%. The net advantage for material costs for single junction modules is approximately 3%.

Labor - No significant difference in labor costs exists between the two types of modules. The labor savings realized for the deposition system is mostly offset by the need to do shuntbusting for single junction modules.

Electricity - Because of the shorter a-Si deposition times, an estimated 7% of electricity cost is saved with the single junction process; this amounts to an approximate savings of 0.4% in material costs.

B. Quality Related Issues

Stabilized Output - In the analysis below, a comparison between tandem and single junction stabilized output is made. However, a complicating factor in comparing modules made at different times, and light soaked at different times and for different durations are the seasonal effects that influence both single junction and tandem modules. In addition, historical light soak data is only available for the older runs that do not have the increased active area developed during this program. Corrections for these factors will be made to the data to develop a fair comparison of the two a-Si options. Averaged data from four tandem runs, which were all measured at the same time, will be compared to calculated values obtained from a model. The same will be done with data from three single junction runs, also measured at the same time. Data is averaged because the process, as well as power output differences between runs, is relatively small and long-term variations are likely to be similar for a given type of module.

It is well known that seasonal fluctuations in a-Si modules exist, although the magnitude can vary from module to module, especially between single junction and tandem, as well as in differing locations and climates. It is also believed that there is a long-term downward trend in output in addition to the seasonal fluctuations. The magnitude of the long-term trend is even more difficult to determine quantitatively, since it is a long-term effect and small on a yearly basis. Nevertheless, there is enough information to estimate the seasonal variations and the longer-term effects by fitting the data to a model. The model used in this study is from Muirhead et al. [2]. In this analysis it is assumed that both seasonal variations and long term degradation are the same for all tandems and for all single junction modules.

The analysis consists of fitting the averaged data to the model by adjusting the input parameters for the best "eye-ball" fit to the data. The calculated values are extended to a 500-day period to show the seasonal variations that might be expected. The equation used to represent the long-term behavior of the modules is the following:

$$P=A*(1+B*\sin(2*Pi*(t/365.25)+C)-D*\ln(t+E))$$

In this equation,

P = power (W)
t = time (days)
A = together with ln(E) the power measured when the module is first placed outside (W)
B = magnitude of the seasonal variations (number)
C= phase factor which takes into account the time of year when light soaking was started (days)
D = long term loss term (number)
E = time related term that describes the initial rapid drop.

The measured averages and calculated values for power output of the modules are shown in Figures 10 and 11.

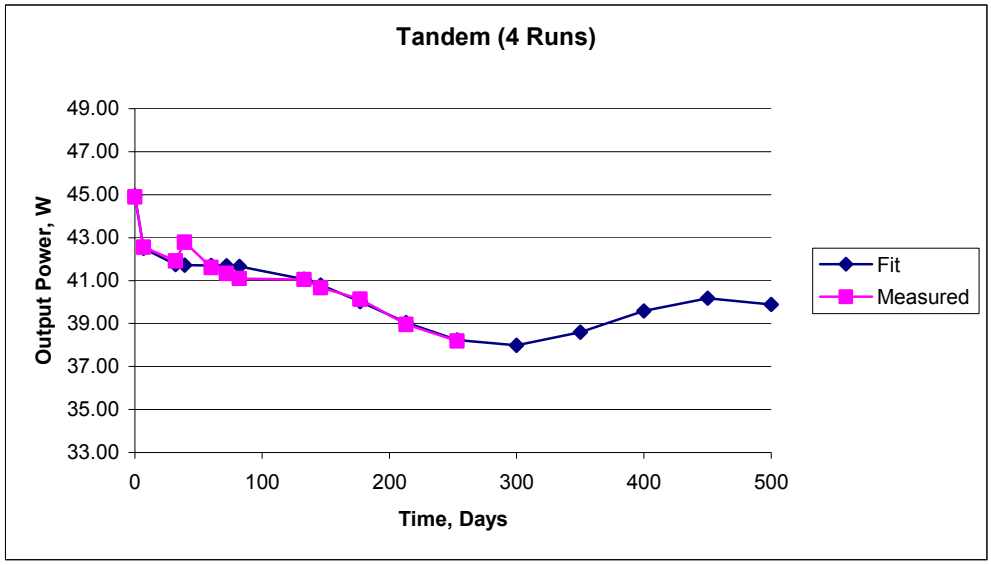

Figure 10: Long Term Performance for Tandem Modules

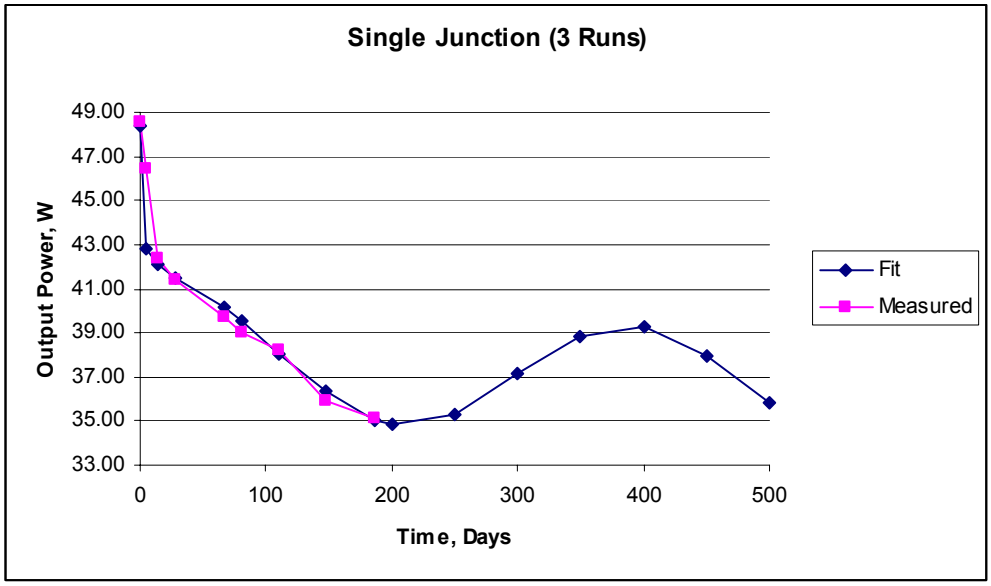

Figure 11: Long Term Performance of Single Junction Modules

The last five measurements were made outdoors for both graphs. Since neither of these groups of modules have the new laser pattern with tighter scribe alignment, a modest 4% higher output is expected for the tandem and 8% for single junction (as discussed under M-1.2.3, larger increases were actually obtained). Adding these amounts, the values given in Table 9 for one year and twenty-year power outputs were calculated. The seasonal and long-term degradation terms used in the calculation are also shown.

Table 9: Comparison of Single Junction and Tandem Long Term Performance

Type	B (Seasonal)	D (Long-Term)	Long-Term Output	
			1 Yr.	20 Yrs.
Tandem	.032	.020	40.6 W	37.9 W
Single Junction	.060	.023	39.9 W	36.7 W

The test modules were in an open circuit condition, so in real applications, somewhat higher outputs are likely to be obtained because the modules would be under load.

Energy Delivery - The total energy delivery for single junction modules was briefly investigated but no firm conclusions could be drawn from that study.

Other Factors

Because fewer layers are needed to make single junction modules, choosing layer thicknesses should not be as critical for single junction as for tandem modules. Thickness uniformity should also not be as critical for single junction modules.

The IV tester flash lamps' spectral output quality is not as critical for single junction as it is for tandem modules.

For a given module area, tandems have a larger active area, because there are fewer cells and hence scribes. Prior to the new layout of the laser patterns, tandems had a 5 to 6% dead area attributed to scribes, compared to over a 10% loss for single junction modules; with the use of a single xy table for scribing all three films, these numbers become a 1.5% loss for tandems and 3% for single junction modules.

C. Performance Summary

Three comparisons have been made between single junction and the tandems. The most important criteria for EPV's current markets is the stabilized output of the modules. The light soak data used in this analysis include only about 10 months of outdoor data but using models to represent seasonal variations, reasonable comparisons between single junction and tandem modules can be made. Allowing for tight scribe alignment, tandem outperform single junction modules by about 3%.

A third, but unknown, factor consists of the gains that are expected in the near future. One area where improvements might be realized in tandems compared to single junction modules is in achieving better uniformity. Since tandems suffer more from non-uniformity than single junctions, the existing non-uniformities, if improved on, will benefit tandems most. More important may be the inclusion of ZnO in the back reflector. As discussed under M.2.4.4, larger gains have been realized for single junction modules than for tandems and this may be sufficient to favor single junctions over tandems for some applications.

A cost related issue, yield, may be different for the two types of devices. No quantitative analysis can be applied at this time, although the higher complexity of making tandem depositions might result in a lower yield. This might be partially offset by the higher complexity of lasering single junction modules.

D. Status

EPV's standard process is for tandem modules. For existing factories, there is a net equipment cost associated with changing from tandems to single junction, because of the additional lasers that would be required. The deposition equipment already exists; hence no saving in this area is possible unless the capacity was increased. The material cost savings alone does not justify changing to single junction, because of the risk that the above uncertainties entail.

The situation may be different for new 5 MW per year factories where a net 12.5% equipment cost savings can be realized for a single junction operation compared to a tandem. This, together with the lower production costs and similar performance, makes the single junction module look attractive, although more reliable and longer-term test data under more varied conditions are needed to form a conclusion.

M-1.2.2 and M-2.2.1 Automated Run Analysis

The main reason for developing an automated batch run analysis is to bring the process knowledge that has been acquired over the years into a single program so that process problems can be detected and corrected quickly. This is particularly valuable to a process manager who may not have extensive process engineering support. In a typical production facility there may be as many as a dozen runs produced in a single day and the early identification of a problem is critical. The intention of the analysis is to have a concise summary of a run that has enough information to not only inform the manager of any problems but also identify their probable cause.

Most data used in the automated run analysis program were generated by the IV tester. Input from other stations is entered manually and the analysis program may prompt the operator for yet additional information.

Because most runs do not have any "problem" plates, a composite run was assembled that included such plates to illustrate how these are identified and classified. Plates are considered "problem" plates if their output is less than 90% of the run average.

The analysis starts with the calculation of averages, i.e.,

- All electrical test parameters (Voc, Isc, etc.) are summarized as a run average and compared to the standard run average
- The same is done with RF sections and plates
- Parameters that are low are flagged
- One of the following choices is then selected by the ARA and printed, depending on the results of the run:
    a. Run is excellent – no problem plates
    b. Run is good – not more than one RF section is poor
    c. Run is mostly bad – more than half the plates are poor
    d. Run is bad – all plates are poor

Except when the run has no low parameters, the sections or plates with low parameters are listed, and possible reasons as well as suggestions for verification given e.g.

Vocs in sections x are below average

the probable reasons in order of likelihood are …

the following tests may more closely identify the problem

Three runs were chosen to demonstrate the analysis - a good run, a bad run and a mostly bad run – this last run is made up to demonstrate a variety of problems. The summary printout that would be obtained for these runs is shown in Table 10.

Table 10: Output of Automated Run Analysis Program

Automated Run Analysis - Summary of three runs		
Run 401	Run is good - all sections are good	
	Sections 2	low Isc
	causes not known	
	determine causes by	
	measure dots - low Jsc or imbalance?	
	determine thickness - too thin?	
	check scribe widths - wide?	
	check RF Current calibration on deposition system	
Run 402	Run is bad - all sections are bad	
	Sections 1, 2, 3, 4, 5, 6, 7, 8, 9, 10	low FF
	likely cause - shorts	
	Sections 1, 2, 3, 4, 5, 6, 7, 8, 9, 10, 11, 12	low Rsh
	Sections 1, 2, 3, 4, 5, 6, 7, 8, 9, 10, 11, 12	low LLL Voc
	Sections 1, 2, 3, 4, 5, 6, 7, 8, 9, 10, 11, 12	low FF corresponds to low LLL Voc
	to verify	
	measure dots - should be good	
	look for pinholes/debris on plate	
Run 403	Run is mostly bad	
	Sections 9	low Voc
	likely causes - shorts	
	Sections 9	low Rsh
	Sections 9	low LLL Voc
	Sections 9	low FF corresponds to low LLL Voc
	to verify	
	measure dots - should be good	
	look for pinholes/debris on plate	
	Sections 4, 5, 6, 7, 8, 9, 10, 11, 12	low FF
	likely causes - shorts	
	Sections 4, 7, 8, 9, 10, 11, 12	low Rsh
	Sections 4, 7, 8, 9, 10, 11, 12	low LLL Voc
	Sections 4, 7, 8, 9, 10, 11, 12	low FF corresponds to low LLL Voc
	Plates 17, 20	low Rsh
	Plates 17, 20	low LLL Voc
	Plates 17, 20	low FF corresponds to low LLL Voc
	to verify	
	measure dots - should be good	
	look for pinholes/debris on plate	
	likely causes is scribes	
	Plates 18, 19, 22, 23, 24	low FF corresponds to high calculated FF
	to verify	
	measure dots -should be good	
	look under microscope, check both beams	

M-2.2.2. Complete Analysis of Impact of Production Downtime and Optimize Production Uptime

In order to maximize manufacturing productivity, an analysis of the pilot line downtime was completed. Information used in the analysis came from data collected over five months of pilot line operation, starting about a month before production began on several large module

orders. Downtime was recorded in approximate hourly increments on a daily basis in an equipment downtime log and then these logs were summarized weekly.

Information is kept on equipment in over 20 different areas of the production process with most equipment having sub-lists of the various downtime categories. The more sophisticated equipment, i.e. deposition and sputtering, contain the most detail. This study examined: 1) the most serious equipment downtime issues facing pilot line production, 2) the benefits of maintaining downtime statistics, and 3) the effect of downtime on a full production line with a nominal 2.5 MW/yr output.

Downtime data - The cumulative data is recorded in a spreadsheet maintained by Manufacturing. In this database, the weekly information is entered for all process equipment. Total downtime hours, total hours available, and total downtime percentage is recorded, and the downtime hours for each of the different equipment areas are summarized.

A five-month cumulative summary with the process equipment areas sorted by highest downtime percentage is the following:

Sandblaster	18.3	Washer	4.3
Deposition	17.2	Bonder	3.8
Sputtering	11.3	Cool – Down	2.6
Substrate carriers	7.5	Laser	2.0
Pre-heat	6.1	Seamer	1.7
Laminator	5.0	Dispenser	1.5
Driller	5.0	IV tester	1.3
Remaining	1.0		

A look at the 'top' 5 categories shows the two most sophisticated systems; the Deposition and Sputtering at the top along with a purely mechanical system, the Sand Blaster. The Sandblaster downtime at 18.3% was unexpectedly high based upon initial expectations. Based on these data, modifications were made to the equipment to improve its operation which has improved its uptime considerably. The recent monthly downtime now averages 1.7%, which is well within the requirement to support a full capacity operation. The Deposition and Sputtering downtime issues are discussed in more detail below in the full production section

Benefits of analysis - There have been a number of benefits to maintaining the downtime analysis and include the following ongoing efforts:

Improved preventative maintenance program (PM) – While an already extensive list of over several hundred PM tasks had already been in use and administered through EPV's PM software system, additional tasks have been added to address some of the equipment issues highlighted by the data.

Improved spare parts, materials, and tools – New materials and tools were gathered and a number of spare parts were procured as a result of the ongoing analysis. In addition a number of recommendations were made for inclusion into the full production line list of materials, tools, and spare parts.

Equipment design recommendations and changes- Several recurring downtime issues prompted review by the equipment design personnel and a number of equipment enhancements were subsequently made.

Improved testing of new equipment and designs- Part of the role of the pilot line is to test new design concepts for the next generation of thin film module production. The improved downtime analysis facilitated this process and has helped in the development of new equipment.

Effect on full production -The production capacity during the period of this analysis was approximately 1.5 MW, which was significantly below the design capacity of 2.5 MW. The reasons for this partially include equipment downtime, but also include factors unrelated to downtime including runs for process and equipment development as well as for business reasons related to product development, materials supply, and timing of orders. However, the data in this study points to several critical areas which could impact the full lines ability to reach its capacity rating. These are discussed in the following sections.

Deposition System – the unscheduled downtime detail by subcategory are listed below:

Section RF	7.7	Pump failure	1.2
No TMB/Silane	3.2	System RF	0.4
TC problem	2.6	Odds and ends	0.2
Vacuum	1.8		

The major downtime issue effecting full production at the a-Si deposition step was the various problems related to the RF generators and section matching networks, shown above at 7.7% cumulative downtime. 2.5 MW production requires 6 full runs a day of 48 plates per run and all 12 sections must be firing and operating for rated capacity to be reached. Since the deposition system is the rate limiting part of the production line, this system would, with the downtime shown, limit the total capacity by a similar amount. As a result of this analysis, the RF problems have been addressed and corrections made to the system. During the subsequent analysis periods after the corrections were made, there was no downtime due to RF problems. The second largest downtime, lack of deposition gas, was attributed to non-recurring human error. As problems are identified and solutions are implemented, these are integrated into the maintenance procedures to minimize future occurrences of downtime.

Sputtering System – the downtime detail by subcategory are listed below:

Target replacement and repair	6.6	Al undercoating	0.4
Vacuum problems	1.3	Chiller	0.3
Pump related	1.0	Vacuum gauges	0.2
Plate jamming	0.8	Drive related	0.2
Gate valve	0.5	Compressed air	0.1

The major downtime issues effecting full production were the various problems related to the target changing process, which had a cumulative downtime of 6.6%. This included the venting of the system, removal of the used target, cleaning of the target area in the chamber, installation of the new target, and putting the system under vacuum to achieve appropriate sputtering vacuum. A number of problems have been revealed in the process not anticipated in the original capacity analysis. This included the number of plates sputtered before the target

change. Originally estimated at approximately 1500 plates, the current lifetime of a target is in the 1000 to 1200 plate range, and thus more target changes are required. The downtime related to the target changes has been reduced by performing this task outside of normal working hours. In addition, various small leaks in the vacuum chambers have contributed to longer pump down cycles before sputtering can begin after a change; these have also been addressed.

Balance of the equipment – The downtime in the balance of the process equipment is not sufficiently high to be rate limiting. Based upon the downtime data currently being accumulated subsequent to the equipment and process upgrades, the pilot line is capable of supporting a full capacity operation.

One important advantage of the EPV process is that the process is a batch process. Since modules travel through the line in 48 plate batches, buffers are used throughout the line to help increase equipment uptime. The effect of the buffer is to decouple a problem in one section of the line from other sections downstream. This provides additional time for the non-rate limiting processes to be brought on-line without affecting the production capacity of the line.

TASKS 2 and 4: STABILIZATION OF PV MODULE POWER OUTPUT

The objective of these tasks was to increase the stabilized power output of EPV's a-Si modules through improvements in device efficiency and optimization of module design to increase the active area of the modules. The task resulted in an approximately 20% increase in stabilized module power output which, together with the reduction in manufacturing cost resulting from Task I, resulted in more than a 25% reduction in the module cost per watt from the Energy Photovoltaics production line.

M-1.4.5 and M-2.4.3 Demonstrate a Total of a 20% Increase in the EPV a-Si Module Stabilized Power Output

Increases in stabilized power output resulted from several milestones in this contract. A brief summary will be presented followed by the individual milestones that are involved.

The optimization and selection of an a-Si deposition recipe was a significant contributor to the increase of stabilized output, although it was not a specific milestone under this program. In early work, a large light soaking study was undertaken, some of the result of which are presented in the comparison of the manufacture of single junction and tandem modules (M-1.1.1). In this study, light soak data was fit to a model that included a seasonal variation in output, presumably due to seasonal temperature changes. By setting the seasonal parameter to zero and calculating the resulting output after one year of outdoor exposure, it was determined that the selected a-Si process resulted in a 5% increase in stabilized power. In terms of stabilized power, modules manufactured prior to this contract were estimated to have an output of 37 W, while the recipe chosen from this analysis resulted in modules with an output of 39 W, a 5.4% increase.

Additional gains were the result of increasing the active area by approximately 8% and including ZnO as part of the back reflector for a gain of approximately 6%. Small gains from improvements in uniformity and tighter process control were not included in the reported total power increase because they are difficult to quantify, but they have a noticeable effect on the

manufacturing process. Combined, these performance improvements result in approximately a 20% gain, and are described in detail in the sections below.

M-1.2.3 - Increasing the Active Area of the EPV a-Si Module Product by 5%

There were three areas in which increases in active area were attained, narrower aluminum foil, narrower scribes and a more optimized layout of the scribe patterns.

Narrower Aluminum Foil - A small gain was obtained from changing the foil width from 6.35 mm to 4.76 mm. This change resulted in an increase in active area of twice (6.35-4.76)/60 or 0.5%.

New Layout - A somewhat larger gain was achieved with an optimized, more symmetrical cell layout. Prior to the change, one of the 38 cells of the module would normally be shorted due to the foil covering parts of two cells. By making both end cells adjacent to the edge deleted strip just slightly wider than the foil and dividing the remaining distance into 38 equally wide cells, a full cell is gained, or 2.7%.

Narrower Scribe Width - The initial attempt to reduce the scribe width focused on improving the tracking of the two xy tables used for lasering, which included an IR laser for tin oxide and a green laser for silicon and aluminum. This was only marginally successful. In some cases improvements of approximately 2% were obtained but they were not very consistent.

To routinely achieve a significantly narrower scribe width, either active tracking using feedback from a microscope needed to be employed or only one xy table had to be used for all three scribes. The latter was used for several runs on a trial basis and was adopted for all lasering. The improved alignment achievable with this approach has resulted in a reduction of the total scribe separation from approximately 0.92 mm to 0.23 mm. The downside of using one the green laser for scribing the tin oxide is that more power or a slower table speed are required (see M-2.3.1 below).

To obtain the area gain from the wider cells, parameters from the xy table control program was used. These show the cell widths to be 16.06 mm before the change and 16.13 mm after. Subtracting the total scribe separation of 0.92 mm and 0.23 mm results in a gain of slightly greater than 5%. A less aggressive tight spacing is typically used in production making the typical gain slightly less than 5%.

Thus the total gain in active area is approximately 8%, 3% of which comes from the extra cell.

M-2.3.1 Demonstrate Automatic Tracking System

Initially, an automatic laser scribe tracking system was to be developed using feedback from a digital camera to control the positioning motor of the xy table. This would allow the laser scribe spacing to be significantly reduced and would increase the active area of the module. However, because of the poor tracking between the two xy tables, the two beams of the dual beam laser scribe process could not be tracked using a single system. As a result, the automatic tracking system based on optical feedback would at best result in half a plate having a larger active area.

A simpler and more effective solution to the problem was discovered when it was noticed that the silicon and aluminum scribes tracked nearly perfectly, to within close to 100 microns. This was because they were both scribed on the same laser station; the scribes remained

parallel even though they were not always perfectly straight. It was determined that the tracking of all three scribes could be achieved if the tin oxide was also scribed on the same laser station. As mentioned above (M-1.2.3), this led to excellent results. After implementing this as the standard process, the throughput decreased because of the slower scribing speed of the tin oxide using a green laser. To increase the production rate, the green laser was replaced with one having twice the output and the number of beams was doubled to four. With this change, not only was a very considerable gain in active area obtained, but also a small net increase in throughput was achieved.

M-1.3.2 Complete Analysis of Higher Quality Tin Oxide Availability and Effect on Product Performance

Module performance has been increased and costs have been lowered through the optimization of the transparent conductive oxide (TCO) front contact. This work was accomplished through a cooperative effort with our tin oxide suppliers.

A total of nine variations of TCO were obtained from our suppliers and tested. The analysis proceeded in two stages starting with single junction modules and then progressing to tandem modules. The data for the two sets of tests are shown in Tables 11 and 12. The "S" prefix denotes a standard product and an "E" prefix denotes an experimental TCO. The two manufacturers used in this optimization are identified as manufacturer 1 (M1) and manufacturer 2 (M2). The standard types of TCO used at EPV are S1-M1 and S1-M2.

Table 11: Single Junction Test Results of Seven Types of TCO, Normalized

TCO Type	Voc	Isc	FF	Power
S1-M1	**1.000**	**1.000**	**1.000**	**1.000**
E1-M1	1.001	1.039	0.989	1.028
E2-M1	0.992	1.024	0.993	1.008
E3-M1	0.996	1.031	0.981	1.007
E4-M1	1.000	1.044	0.998	1.021
S1-M2	**1.006**	**1.054**	**0.978**	**1.036**
E1-M2	1.009	1.000	0.982	0.990

Table 12: Tandem Junction Test Results of Nine Types of TCO, Normalized

TCO Type	Voc	Isc	FF	Power
S1-M1	**1.000**	**1.000**	**1.000**	**1.000**
S2-M1	0.997	1.010	0.980	0.986
E1-M1	1.005	1.043	1.000	1.048
E2-M1	1.006	1.039	0.982	1.027
E3-M1	1.001	1.035	0.994	1.029
E4-M1	1.003	1.039	0.988	1.029
S1-M2	1.005	1.053	0.976	1.033
E1-M2	1.010	1.044	0.970	1.023
E2-M2	1.015	1.049	0.985	1.049

In the single junction study, it was observed that the standard product S1-M2 TCO outperformed all other types of TCO. However, several manufacturers of PV products including EPV noticed that this TCO was sometimes prone to delamination and therefore was not suitable for use in production [3]. By cooperatively working with the supplier, alternatives were developed that did not have this problem. The first experimental TCO from this supplier (E1-M2) was shown not to delaminate, but it did not perform as well as other products in single junction tests. Meanwhile the other supplier developed four variations of their TCO, two of which looked promising (E1-M1 and E4-M1).

In the second stage of testing, tandem modules were tested on these same TCO varieties with the addition of a new improved version from manufacturer 2 (E2-M2), and a second standard product from manufacturer 1 (S2-M1). The results on standard tandem modules were very encouraging. Two types of TCO emerged as being superior to the previous standard products. The new type E2-M2 was 4.9% better than the reference TCO, followed closely by E1-M1, which was 4.8% better. In addition, all of the experimental TCO types were shown not to delaminate during testing.

Manufacturer 2, convinced of the improvements made in their latest version of this TCO, made the E2-M2 TCO their standard product. Subsequent modules made on this TCO have demonstrated their robustness in preliminary outdoor exposure tests and so this was adopted as an EPV pilot line standard TCO. Concurrent with the TCO optimization, EPV negotiated a 23% cost reduction for this TCO.

M-2.1.2 Improve Uniformity by Optimal Combination of Process Conditions and Improvements in the Deposition System

The thickness uniformity of the a-Si film is important for two primary reasons, performance and aesthetics. A uniform plate can be optimized for maximum power over the entire area of the plate, whereas a non-uniform plate will have regions that perform more poorly, and thus bring down the average performance. In the most severe cases of non-uniform a-Si, the plate can develop shunts and significantly pull down the power output of the entire plate.

Uniformity is also important to ensure a uniform appearance of the module. As the thickness of the a-Si layer changes, the reflected color of the module changes as a result of the interference fringes produced by the thin silicon layer on the tin oxide. A difference of several hundred angstroms in a-Si thickness can be easily seen on a module, especially when there is an abrupt change in thickness. Appearance is not important for some applications since the modules are not visible after installation, but for other applications, the appearance is critical. It is particularly important in building integrated PV (BIPV), a market in which the uniform appearance of a thin films product is a major selling point.

To help determine a-Si uniformity over large areas, a means was sought to quickly quantify the silicon thickness without damaging the plate. The standard methods of determining thickness were to use a profilometer to measure thickness directly or to measure the capacitance of a small cell of a known area. Both of these methods have the drawback of destroying the plate in order to obtain the measurement. In addition, they are both time consuming, which discourages their use for large uniformity studies.

Since the goal was to assess the a-Si film uniformity, it was determined that an absolute measurement was not required; a repeatable technique that would provide relative thickness contours over a plate would suffice. As a result, a quick reliable technique was developed to measure thickness based on the reflected color of the film. This approach had the benefit of acquiring data very quickly without destroying the plate, and provided sufficient data points to allow mapping the uniformity of a plate relatively easily.

The technique developed involved accurately quantifying the appearance of the a-Si by measuring the intensity of reflected light using a handheld spectrophotometer. Since the thin a-Si film reflects light from the top and bottom surfaces constructively and destructively based on the thickness of the film and the wavelength of light, by precisely characterizing the reflection spectra, it is possible to empirically correlate the appearance of the a-Si with thickness.

Figure 12 shows a typical reflectance spectrum for a sample of a standard tandem a-Si/a-Si module that is approximately 5000 Å thick. The reflectance spectrum is measured from 400 nm to 700 nm in 10 nm increments using a portable Minolta CM-508d spectrophotometer with D_{65} illumination (average daylight light source including UV).

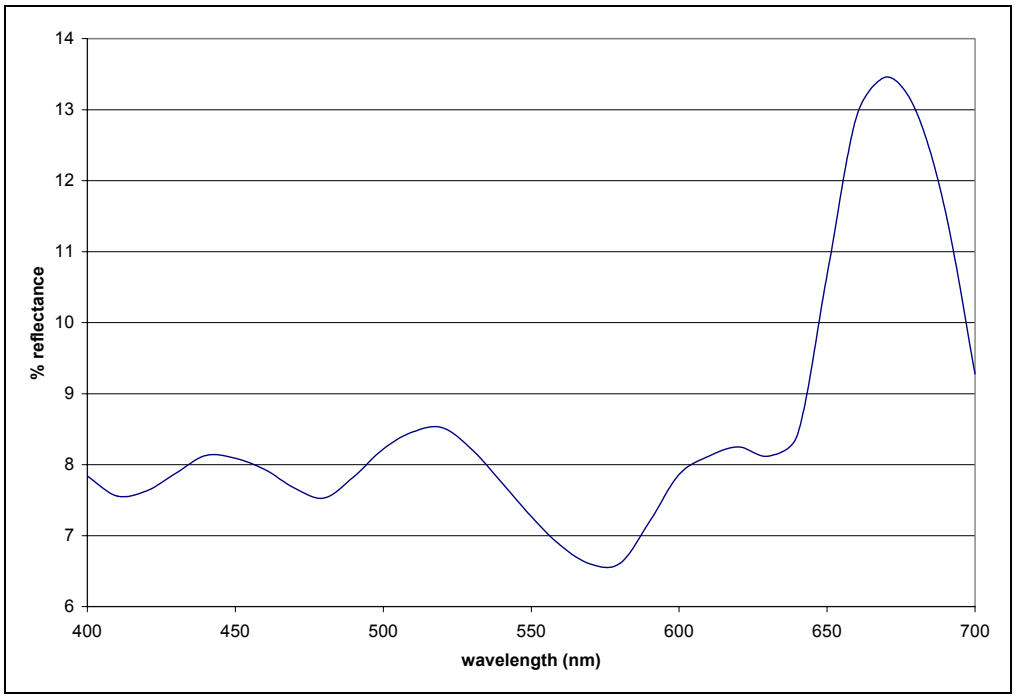

Figure 12: Reflectance Spectrum for a 5000Å a-Si Tandem Module (289-16)

By accumulating many spectra similar to the above and measuring the corresponding a-Si thickness on each sample using a profilometer, an empirical model relating spectral information to thickness was developed. Parameters for the model were obtained from a linear regression using only the statistically significant wavelengths. The correlation between measured and calculated thickness is shown in Figure 13. The typical deviation from the fit in this model is about the same magnitude as the profilometer repeatability.

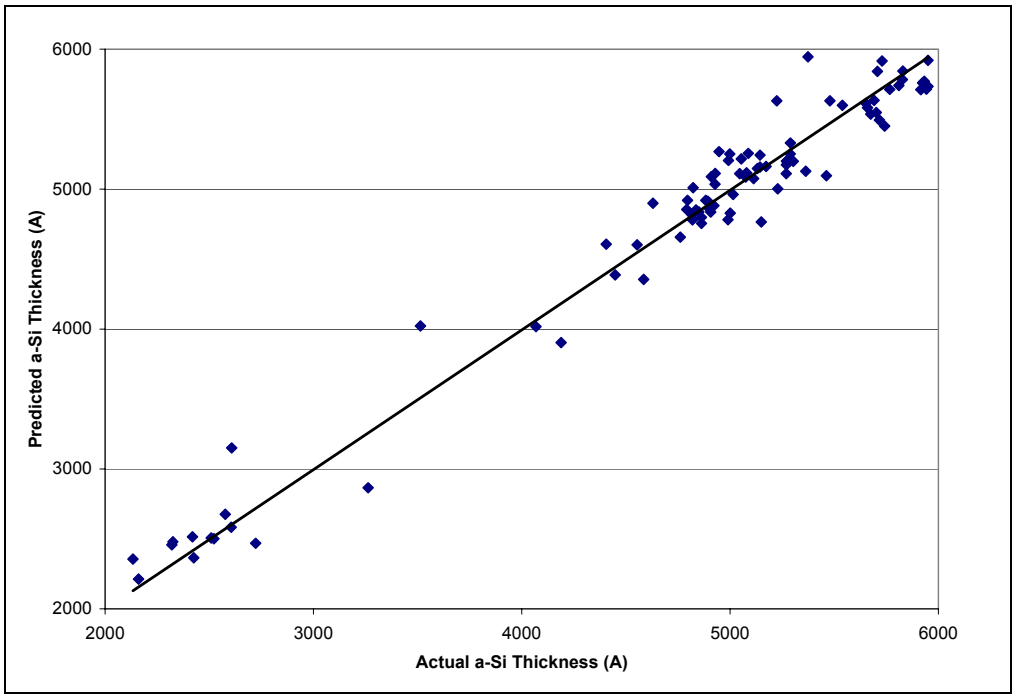

Figure 13: Predicted vs. Actual a-Si Thickness using Model Based on Reflection Spectra

The first use of this non-intrusive optical technique for measuring thickness was to compare the uniformity and repeatability of the plates in consecutive runs. To help visualize the uniformity, contour plots of the thickness were generated. Three plates were analyzed, which were deposited in different runs but were made in the same substrate carrier and in the same position in that carrier. This ensured that for each plate the same electrodes and plate-positioning guides were used; any variations in the plates should be due to run dependent factors and not due to variations in system geometry. In order to begin to understand the effect of position on uniformity, plates were also evaluated that were in the same run, but were located in adjacent RF sections.

The contour plots in Figure 14 show the uniformity maps for three plates deposited in substrate carrier 'A' position 43; each plot is generated from measurements at 90 points over the plate. Plates 318-43 and 320-43 are consecutive runs for substrate carrier 'A' and the similarity in uniformity is clearly evident. The average thickness for these plates is essentially the same within ~2%, which is less than the average scatter for the optical thickness measurement technique. Plate 294-43 was manufactured nearly a month prior to runs 318 and 320 using substrate carrier 'A', but the thickness variation is very similar to the later plates in position 43. For all three runs, the range of thickness variation is approximately 13%, with the thickest regions along the long edges of the plate. This seems to indicate that the uniformity variations are predominantly caused by fixed factors that are related to equipment and process variables, and not to changing conditions imposed by the operator or feedstock materials. The plates made in consecutive runs show less than 1% variation in average thickness, which indicates the excellent short-term reproducibility of the process.

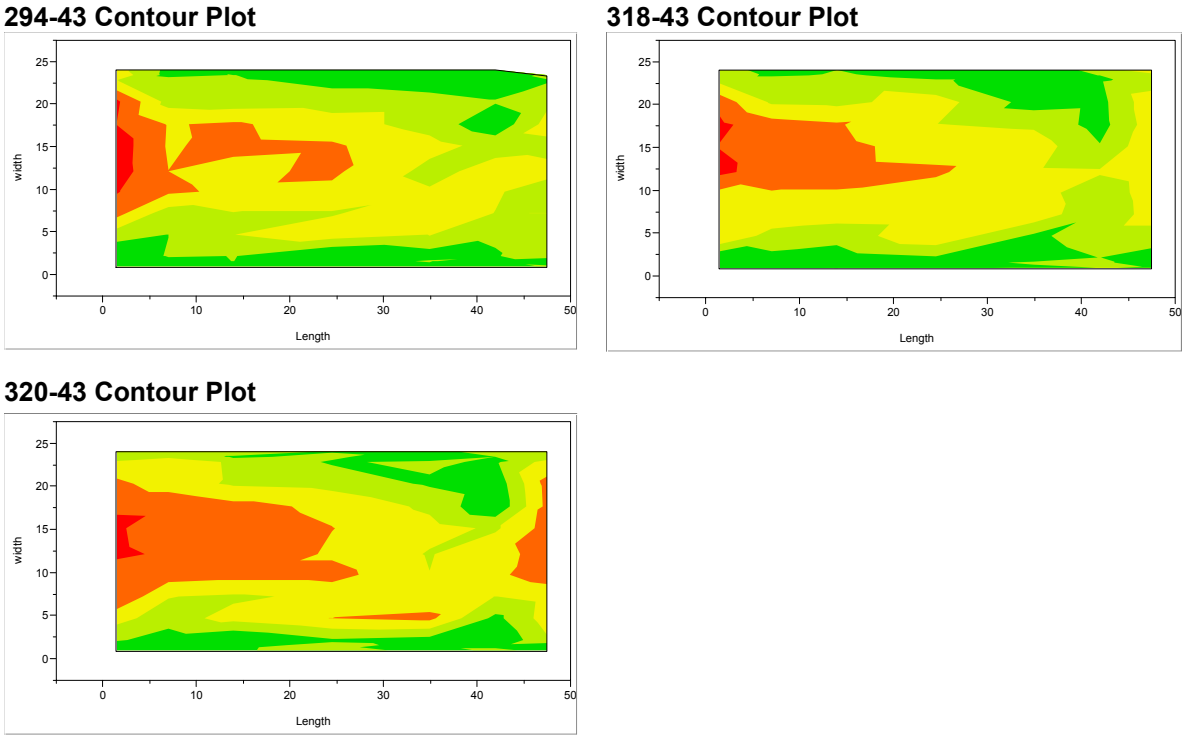

Figure 14: a-Si Uniformity of Plates in the Same Plate Position in Substrate Carrier A

Contour plots from other substrate carriers show very different uniformity contours. This can be seen from the difference in uniformity shown in Figure 15, which describes the uniformity of the a-Si in the same plate position, but in a different substrate carrier (B). This difference seems to indicate that there are significant factors affecting uniformity that are related to physical parameters in each substrate carrier. These factors may include differences in plate positioning, electrode spacing, and local gas flow patterns.

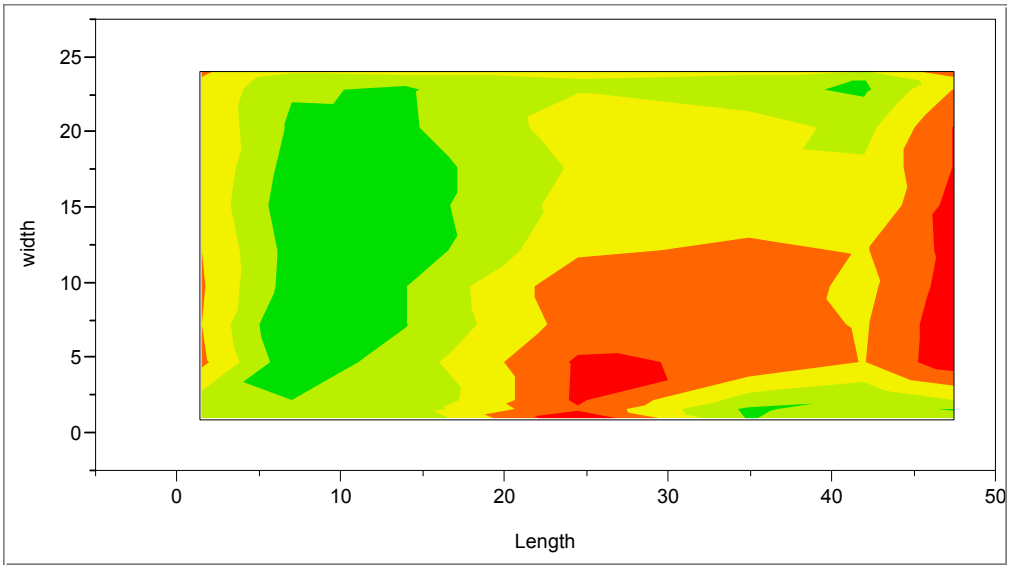

Figure 15: Average a-Si Uniformity for Position 43 in Substrate Carrier B

To determine the effect of differences in matching networks, power supplies, and control systems on uniformity, these components were switched between sections. These changes had no apparent effect on uniformity. The RF feed point to the electrode was modified resulting in some improvement, but the major non-uniformities still persisted. To determine if the power level during deposition could improve the uniformity, a deposition was made in which the power level was modulated +/- 8%. The resultant plot did not indicate a major change in uniformity. The effect of gas flow was tested by increasing the total gas flow by 45% across the plate during deposition. Again, the uniformity of the a-Si did not significantly change beyond the detection limits of the measurement technique. The temperature uniformity of the substrates was also modified with no apparent effect on uniformity. These experiments and others like them lead to the conclusion that the physical factors affecting the plasma uniformity, such as electrode spacing, were likely the dominant factor affecting a-Si thickness uniformity.

To narrow in on the areas where thickness variations were most prominent, uniformity mapping was carried out for most of the positions in a 48 plate a-Si run. These were analyzed individually and together in combination with other plates. The plates that faced the same plasma were compared with those in adjacent RF half-sections, which share the same power supply and matching networks, which were in turn compared to plates made in adjacent sections, which have no common elements other than the process chamber and gas feedstock.

Individual Plate Variations – The analysis of the uniformity contours for individual plates indicated that there were a wide variety of patterns throughout the entire substrate carrier. It was evident from a quick review of the maps that there was no particular pattern common to all plates that may have indicated a system-wide factor that affected uniformity on a global scale. The wide variety of patterns seemed to indicate that the most significant variations were at the plate level and not due to system-wide deposition conditions.

Half-Section Variation - In contrast to uniformities of plates that are not opposed to each other, it was found that plates that were deposited in the same half-section, e.g. plates that share the same electrode-ground pair, have uniformity patterns that are mirror images of each other. This is expected, since plates in the same half-section face each other with the same plasma between them during deposition, and therefore any process non-uniformity affects each plate equally. These uniformity maps provided evidence that the plasma uniformity is a key factor in the a-Si uniformity of a plate, and variables that influence the plasma uniformity, e.g. geometry of each plate position, RF conditions, etc., are expected to change the deposition uniformity.

RF Section Variation - To determine the effect different RF sections have on uniformity, the thickness uniformity for all plates in each section was averaged, and this was compared to the averages for the adjacent RF sections. As expected, the amount of variation between RF sections was found to be larger than the variation within a section, or a half-section, but significantly less than the variation within a single plate. A summary of the amount of variation in each of these cases is shown in Table 13.

Table 13: Comparison of Average Thickness Variations in a Single Run

Comparison	Range of Thickness
variation in avg. thickness in adjacent plates (same half-section, same run)	1.2%
variation in avg. thickness in adjacent half-sections (same section, same run)	3.4%
variation in avg. thickness in adjacent sections (same run)	5.0%
avg. thickness variation within a single plate	14.3%

It is clear from these data that the amount of variation in uniformity caused by RF section differences is low (5.0%). The amount of variation on a single plate is nearly tree times as large, on average (14.3%). This once again indicates that variables specific to a particular plate position are likely to be responsible for most of the non-uniformities in the deposition system. These results also show that differences that affect RF section uniformity, such as power supply calibration and matching network tuning, are not significant contributors to plate non-uniformity. This is evidence that the scheduled maintenance of the a-Si deposition system is effectively preventing these factors from becoming problems.

To demonstrate the effect that spacing has on deposition uniformity, several experiments were run to simulate warped electrodes and glass spacing variations. One of these is shown in Figure 16. In this experiment, a 3 mm thick glass spacer was inserted behind the glass substrate and a standard deposition was run. It is very apparent from the figure that there was no deposition in the center of the substrate where the spacer was placed. In this extreme case, the uniformity of the plasma was severely affected to the point of extinguishing in the middle of the plate.

Figure 16: Effect of Glass Spacer between Electrode and Glass Substrate

To determine any effect that electrode spacing variations may have on the manufacturing process, the spacing uniformity of the electrodes was measured and correlated to historical process line yields. It was discovered that the variation of substrate carrier A was more than twice the variation of substrate carrier B, and the dropout rate, due to low power, for substrate carrier A, although small, was 34% higher than for B. This correlation, although anecdotal, was consistent with the other evidence indicating that the electrode spacing uniformity was responsible for the observed variations in a-Si thickness.

In light of the data accumulated to this point, it was decided to improve the substrate carrier design to reduce the variation in electrode spacing. The internal parts of the substrate carrier were modified and/or redesigned with the most significant change being the electrode plate. The original electrodes were made from standard mill stock material with wide tolerances on flatness. In the new design, flat jig-plate grade material was specified to ensure minimal warpage. The upgraded substrate carrier was assembled and the electrode plates could be seen to be visibly flatter. After some optimization of the process, test plates were evaluated and contour maps were plotted. The result of the improvement is shown in the representative plates shown in Figure 17. Each of these plots is based on thickness data from over 244 points over the entire plate. As can be seen on these contour plots, there is a distinct improvement in the uniformity, especially in the middle of the plate. There are still some non-uniformities on the edges and near the RF-feed point, but these are expected to be reduced through further modifications. However, it appears that the flatter electrode plates significantly improve the deposition uniformity.

Before equipment modifications (standard deviation = 5.7%)

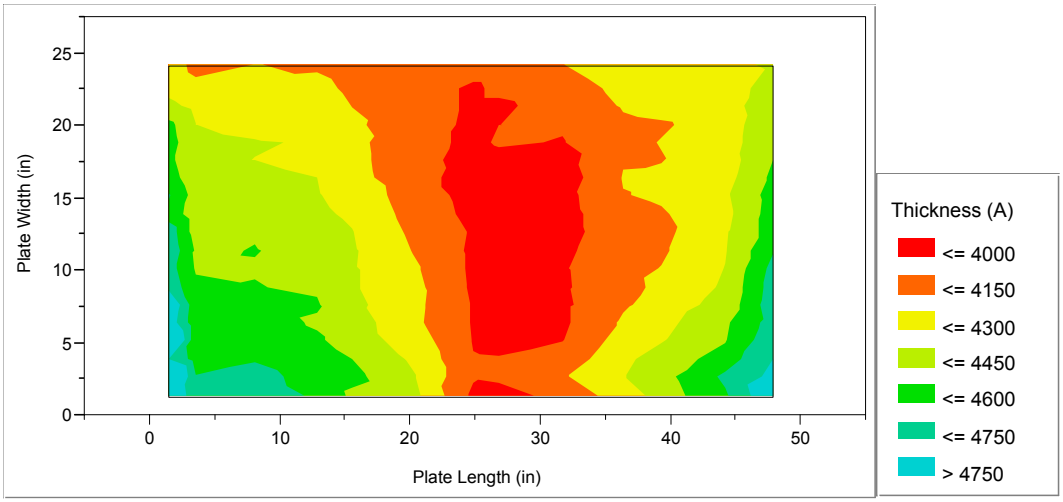

After equipment modifications (standard deviation = 3.3%)

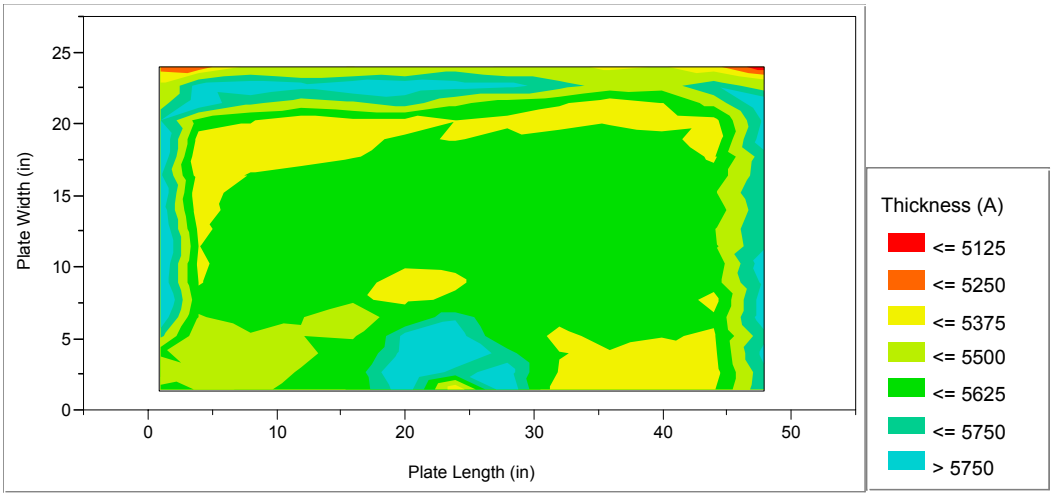

Figure 17: Representative a-Si Thickness Uniformity Plots before and after Equipment Modifications

M-2.4.4: Complete the Identification and Evaluation of a New Back Reflector for the Use in the Production of EPV a-Si Modules

In an effort to improve module efficiency, the benefit of using a composite zinc oxide–aluminum (ZnO/Al) back contact has been investigated. EPV's standard back contact has been sputtered aluminum, which does a good job of collecting current from the a-Si at a reasonably low cost. However, it is well known that by inserting a transparent conductive oxide between the aluminum and the a-Si, the reflectivity of the back contact can be significantly improved [4].

A. Preliminary Small Area Studies

The investigation began by using small test samples of a-Si cut from full sized plates produced in the pilot line. Samples with the same a-Si were cut to approximately 5 cm x 10 cm, and each of these was processed with either the standard back contact, Al only, or a sputtered ZnO/Al back contact using a small research sputtering system. For the initial tests, single junction a-Si was used to simplify the data analysis. Small area devices were formed on these samples using an etching procedure and the QE currents were measured. A typical result is shown in Figure 18.

These initial tests show that the long wavelength response of the a-Si can be significantly improved by using a ZnO/Al back contact. The QE curves in Figure 18 show that the Jsc for the ZnO/Al sample is 8.7% higher than the Jsc for the sample with the Al back contact. As the figure shows, this improvement comes from an increased long wavelength response, mainly between 550 and 750 nm. The ZnO clearly improves the reflectivity of the back contact resulting in greater absorption of light in the active semiconducting layers. This initial result was encouraging and further optimization was pursued to develop a process suitable for large-area modules.

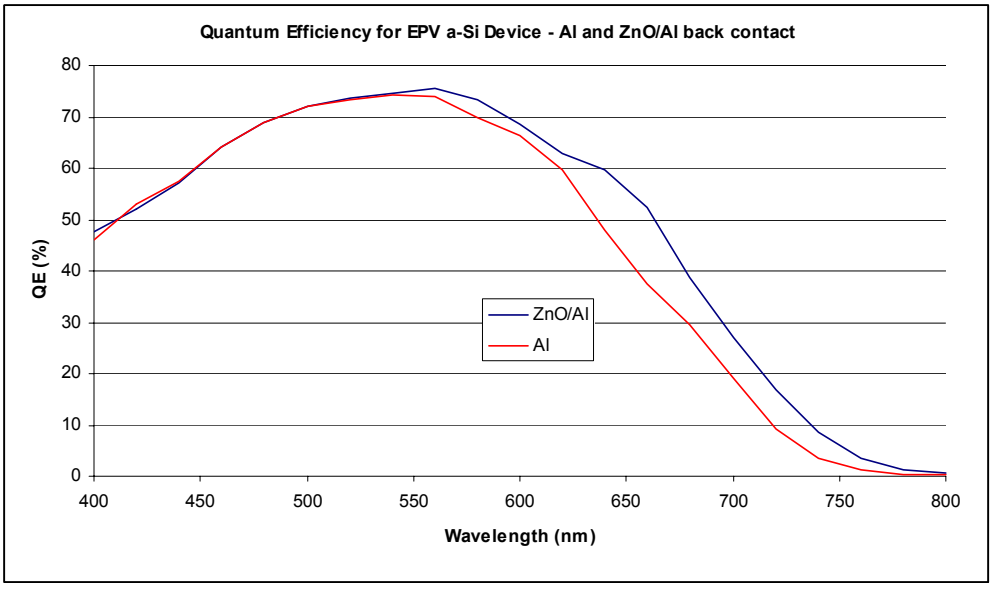

Figure 18: Quantum Efficiency Curves for Single Junction a-Si with and without ZnO Back Reflector

In an effort to characterize the sensitivity of the current gain with respect to variations in ZnO thickness, a second series of experiments was conducted in which the ZnO thickness was varied from 0 to 1600 Å and the Isc was measured for each small area cell. Once again, the same single junction silicon was used from the EPV pilot line to simplify the characterization. The results are plotted in Figure 19, along with a best-fit polynomial curve.

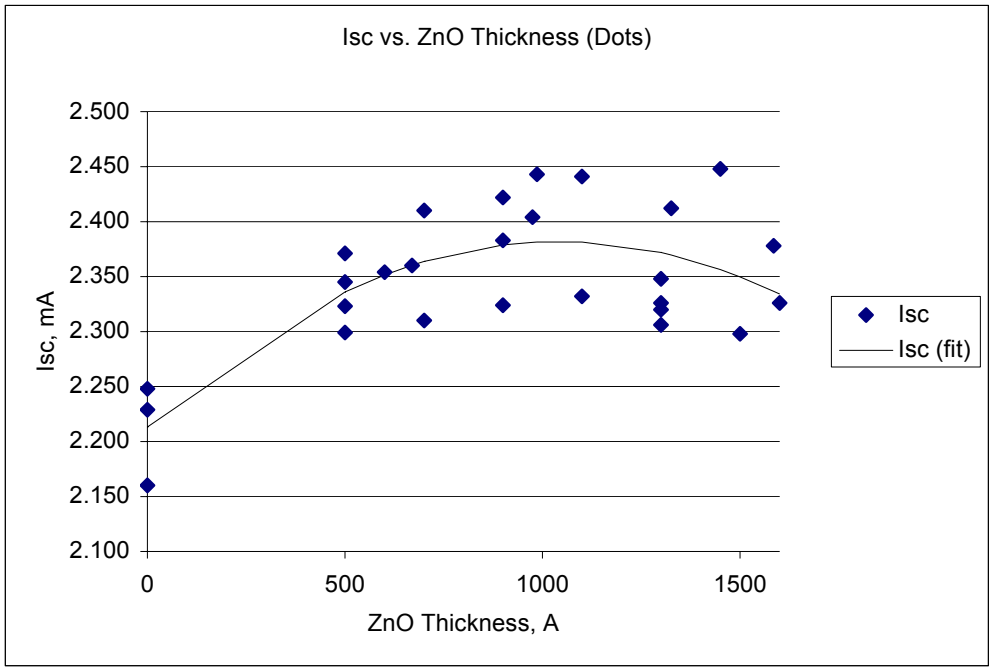

Figure 19: Small Area Cell Isc vs. ZnO Thickness on Single Junction a-Si

The data in Figure 19 show that the presence of ZnO has a significant effect in increasing the cell Isc. The control samples with no ZnO have the lowest Isc and it appears that initially the Isc increases with increasing ZnO thickness. Near approximately 1000 Å (±~100-200 Å), the increase seems to level off with increasing thickness, possibly saturating. Beyond ~1200 Å, the data seem to show a possible decrease of Isc with increasing ZnO thickness, however, the scatter in the data does not allow determination with any certainty whether the Isc drop observed in this experiment is statistically significant.

While it is clear that there is significant variation in the data, and thus the precise placement of the curve is subject to some uncertainty, it can be seen from the general shape of the curve that the Isc is not very sensitive to variations in the ZnO thickness. The peak centered around ~ 1000Å is very broad, which indicates that large variations on the order of ±20% have little effect. This is an encouraging result that helps ensure high process yields when the ZnO process is used in a manufacturing environment.

The overall improvement in Isc is also very encouraging. If the best fit curve is used to estimate the Isc of a typical sample with a 1000 Å ZnO back reflector sample, it can be estimated that the Isc is expected to be 7.7% better than the controls, a result in line with the previous experiments.

B. Initial Submodule Testing

To develop a process suitable for large-area modules, a pulsed DC sputtering system was used which was capable of depositing ZnO on substrates that are 48.25 cm x 91.5 cm (19" x 36"). The work began on this system so that the information needed to retrofit the production sputtering system for full sized plates could be obtained. Once again, to simplify the analysis, single junction a-Si from the pilot line was used for the experiments. These tests demonstrated the scalability of the process, and provided a means to optimize the a-Si and laser scribing processes. Performance gains of greater than 7% were achieved.

C. Evaluation of Interconnect Region

Having established the gains achievable with a ZnO/Al back reflector, the interconnect integrity was examined next. In order to incorporate the ZnO into a module, it was necessary to determine whether the presence of ZnO in the interconnect region would cause any performance or reliability problems. If the ZnO had no effect in the interconnect, then the ZnO could be deposited after the a-Si scribe and during the same process as the Al sputtering. However, if the ZnO harmed the interconnect, then it must be deposited before the a-Si scribe, and it would requires a separate sputtering step separate from the Al, a more expensive process sequence.

To evaluate the reliability of the interconnect, mini-modules, ~5 cm x 10 cm, were fabricated using the same a-Si and ZnO deposited in the small-area ZnO system used for the previous tests. The experiment was divided into three groups: 1.) control plates with Al back reflectors and no ZnO, 2.) ZnO/Al back reflector plates with ZnO filling the interconnect scribe, and 3.) ZnO/Al back reflector plates with Al filling the interconnect scribe.

One sample from each of the three groups was thermally cycled between -10°C and 30°C; each cycle included at least 24 hours at –10°C. At regular intervals during the cycling, the interconnect resistance was measured across a single segment on each sample to determine if the interconnect was being degraded. Particular attention was paid to the sample that contained ZnO in the interconnect scribe to determine if the thermal cycling would open that connection and consequently result in high resistive losses. Over the course of 12 thermal cycles, the interconnect resistance was unchanged for each of the samples, within the measurement error. Based on this result, it appeared that interconnects filled with ZnO are equivalent to interconnects filled with Al on ZnO back reflector modules when subjected to moderate thermal cycling.

At a later date when the large area sputtering system was operational, the effect of ZnO in the interconnect was once again tested. Modules were produced that had ZnO filling the interconnect and were compared to similar modules with Al in the interconnect. It was found that the modules with ZnO in the interconnect had lower fill factors (FF) due to an increased series resistance. It appeared that the higher resistivity of the ZnO, as compared to the Al, was large enough to affect the internal resistive losses of the plate. The lower FF offset the operational advantage of sputtering the ZnO after completing the a-Si scribe, and therefore the higher performance process was adopted as the standard ZnO/Al sequence.

D. Production Line ZnO/Al Back Reflector Module Development

Based on the success of the small area cells and submodules, the production Al sputtering system was modified to deposit ZnO on full-sized 25" x 49" (0.79 m^2) modules. A 99.9% purity target with the composition of the target that used in the small area tests, 98% ZnO / 2% Al_2O_3, was specified to keep material costs low.

The large-area production worked very well and good quality ZnO films were produced with good uniformity. The ZnO films tested were in the thickness range of 200-1600Å with a resistivity of 2 - 4 x 10^{-3} ohm-cm. The nominal process was typically approximately 1000Å thick with a sheet resistance of about 200 ohm/square.

The qualitative uniformity of the ZnO was very good as could be plainly seen by the color uniformity of the ZnO interference fringes on the a-Si. A light blue/pale yellow color was visible in the center of the plate and this gradually transitioned to a deep blue on the edge where the ZnO was thinner. The thickness of a test film was measured across the width of a substrate and the uniformity data of a typical ZnO film is shown in Figure 20. The thickness of the middle 70% of the plate is within 7% of the thickest point located in the center of the plate, and the thinnest point on the edge is only ~20% thinner than the center. As discovered in the earlier tests, the ZnO thickness can vary significantly and still yield excellent results, as shown in Figure 19. The variation of ZnO thickness described by Figure 20 is more than sufficient uniformity for a high performance back reflector.

The optimization on full-sized modules again began with tests on single junction a-Si so that the effect of the ZnO could be easily determined from module IV data. A series of thin i-layer single junction plates was deposited in a single run and was processed with varying thicknesses of ZnO. The results are shown in Figure 21.

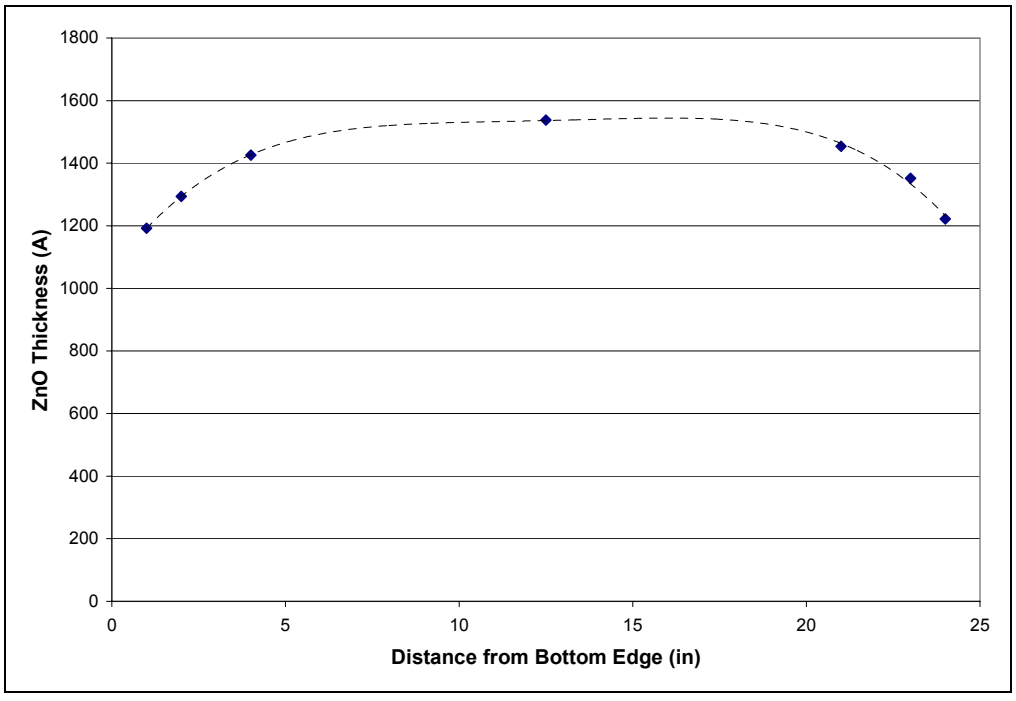

Figure 20: ZnO Uniformity across the Width of a 25 inch Substrate

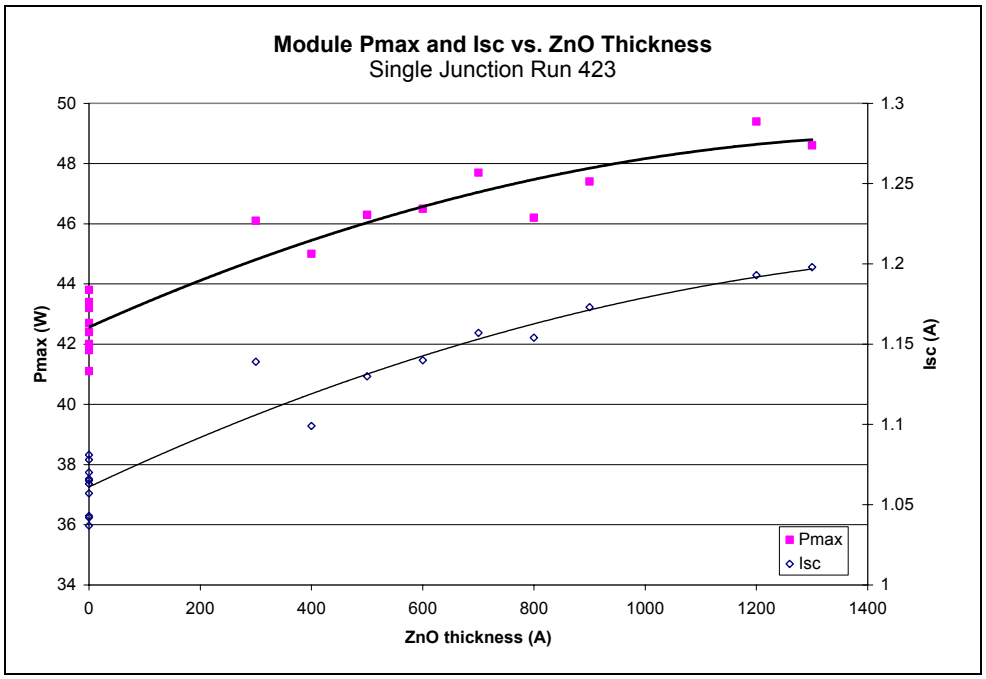

Figure 21: Effect of Increasing ZnO Thickness on Thin i-layer Single Junction a-Si Modules

The data above shows a direct correlation between ZnO thickness and module Isc. As the thickness of ZnO increases to >1000 Å, the Isc increases by ~10-12%, a significant improvement. The trend is similar to the small area results shown in Figure 19, but it is encouraging to note that the increase in current is higher in these recent module tests than in the small area tests where a 7-10% improvement was observed.

The improvement in module power follows the same trend as the Isc, which indicates that any deleterious effects of the ZnO on the module Voc and FF are minimal. The average increase in power for modules with at least 900Å of ZnO is 13.2%, and the best module increased 15.7% with the inclusion of ZnO in the back reflector. These test results imply that the ZnO/Al back reflector offers a significant improvement in performance for single junction modules, in fact, the performance improvement is larger than has been observed in initial tandem a-Si experiments. This may suggest that, in some applications, a single junction module with ZnO/Al may be preferable to a tandem. Experiments with tandem junction modules resulted in a similar, but thinner optimum ZnO thickness, ~900-1100Å.

Using the ZnO thickness information from previous experiments, the tandem process development could proceed, beginning with the i-layer optimization. The process of implementing an enhanced reflector in a tandem device is complicated by the requirement that each junction must generate about the same amount of current in order for the full benefit of the improvement to be realized. Since most of the additional light reflected by the ZnO is toward the red end of the spectrum and is absorbed by the back junction, the front junction needs to be made thicker in order to maintain the current balance and optimize performance. Several sets of runs were completed with varying i-layer thicknesses. The most significant results of the optimization are shown in Figures 22 and 23.

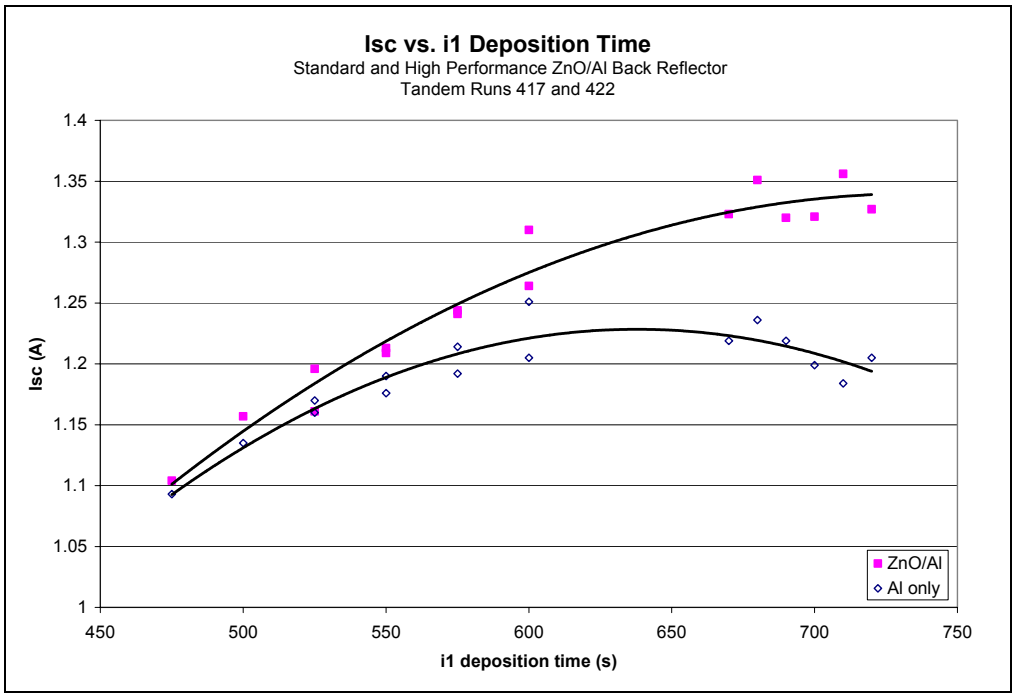

Figure 22: Effect of ZnO/Al Back Reflector and i1 Deposition Time on Isc of Tandem a-Si Modules

It is evident from Figure 22 that the optimum i1-layer deposition time, i.e. i1 thickness, is different for the two cases shown. For the standard tandem, without ZnO, the maximum current is generated in the 600-680 second range. As i1 becomes thicker, the device starts to become back limiting as excessive light is absorbed in i1, depriving i2 of light, resulting in lower Isc. However, with the enhanced back reflector, i2 is not limited with the thicker i1 layers used in these experiments and the resultant Isc of the module continues to increase with i1 until it is about 8% greater. The Isc maximum is pushed out to a thicker i1, which appears to be somewhere above 700 seconds.

This effect is even more dramatic on the module power plot, Figure 23. Once again, the standard tandem reaches a maximum in the 640-680 range, and the performance decreases beyond that range with thicker i1. However, the modules with ZnO continue to improve with thicker i1, with a maximum that appears to be somewhere well beyond 720 seconds. The typical improvement in performance in this experiment is similar to the improvement seen in Isc, at about 8%.

Based on the process developed in these experiments, larger scale pilot productions runs were completed which used a 900-1100Å ZnO layer in the back reflector along with a thicker i1 layer. The performance of the ZnO modules was increased by an average of 7.4% with most of the improvement coming from the Isc, as expected. Since some of this gain may be lost during stabilization, a 6% net gain is expected from the use of a ZnO/Al back reflector. The IV data for the two modules sent to NREL as deliverables is shown in Table 14

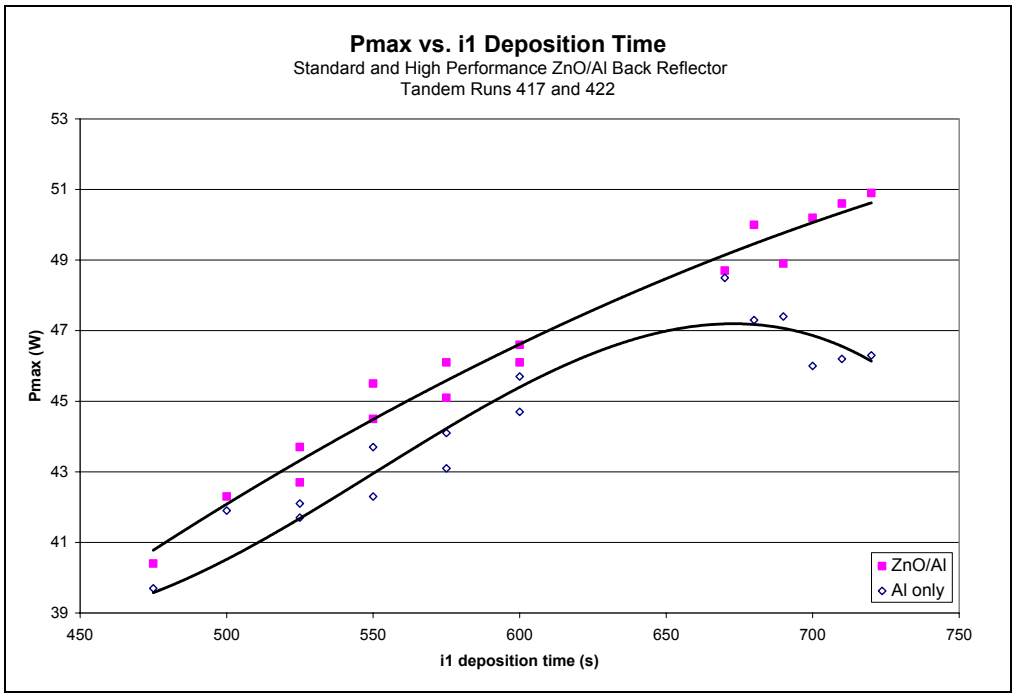

Figure 23: Effect of ZnO/Al Back Reflector and i1 Deposition Time on Pmax of Tandem a-Si Modules

Table 14: Initial IV Data for Modules Incorporating the Optimized ZnO/Al Back Reflector

	Modules with ZnO/Al back reflector	
	503-12	**503-22**
Voc, V	58.8	59.1
Isc, A	1.370	1.322
FF, %	63.3	64.8
Power, W	51.0	50.7

Measurements

It is critical to develop measurements that reflect the performance of modules under real-world conditions. However, it is impractical to rely on outdoor measurements for routine characterizations of PV products, for a variety of technical and logistical reasons. In an effort to more closely predict the outdoor performance of modules, the characterization methods for measuring both the initial and stabilized performance of EPV's modules were improved.

A. Comparing Indoor and Outdoor Measurements

To calibrate outside measurements, a series of comparisons was made over a period of approximately a month in which eleven modules were repeatedly measured both indoors and outdoors. Indoor measurements were made with the flash tester calibrated with a NREL measured module and outdoor measurements with a portable IV tester using a small

photodiode as reference. The purpose of these measurements was to obtain an estimate of the reliability of outdoor data and to calibrate the reference cell used outdoors. Light-soaked single junction and tandem modules and non-light soaked single junction and tandem modules are included in the comparison. The first comparison indicated that the photodiode reference value resulted in modules having an output approximately 4% too high – this was corrected. Temperatures, both of the modules and the reference cell were also investigated.

Module temperature - Even with no uncertainty in the reference cell, there is some uncertainty in the module temperature. The module temperature is measured on the front or back surface, but the film temperature is not known. This is not necessarily a problem as long as the temperature measured is meaningful and stable. Unless modules are being light-soaked, outdoor exposure time during a measurement is usually held to a minimum and modules do not necessarily have time to equilibrate in temperature. This causes the temperature of the module surface and the inside thin films to not be precisely related. The magnitude of the effect on measurements was determined experimentally. Figure 24 shows Voc values taken 0.4 seconds apart for 400 seconds. Attempting to fit the voltages to a single exponential decay resulted in poor agreement but two exponentials described the decay well as shown on the graph.

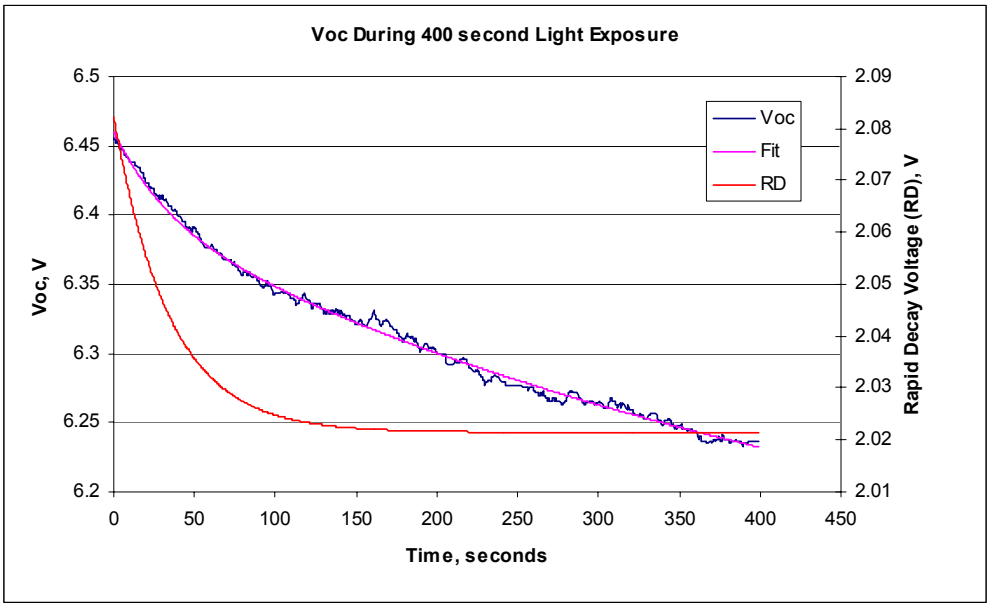

Figure 24: Change in Voc as Function of Time Exposed to Sun

The two exponentials have time constants of 34 seconds and 530 seconds. The rapid decay, shown in the graph as RD, corresponds to a voltage drop of approximately 1%, implying an approximate 3ºC temperature rise in 100 seconds. This temperature rise can reasonably be assigned to the initial temperature rise of the thin film. The slower decay amounts to approximately 5%, or 16ºC, and is very likely due to the slower heating of the module glass. The rapid decay time-constant is of the order of the variation in the time required to position the module outside, make electrical connection, etc., and could therefore account for nearly 1% in Voc variations. To minimize errors resulting from these effects, an effort is made to keep the outdoor exposure the same for all modules measured.

Reference cell temperature - When measuring modules outdoors, IV parameters, front surface module temperature, and photodiode output but not its temperature, are measured. Typically the output of a photodiode is either measured as a current or as a voltage across a load resistor. In either case, the operating point of the diode will be low enough to effectively measure the short circuit current. This current will be temperature dependent. Because temperature coefficients for current and voltage have opposite signs, using a higher operating point than typically used should result in a lower, possibly even zero, temperature coefficient. Tests were carried out to determine the extent to which the temperature sensitivity could be reduced. Figure 25 shows the output current of a 1 cm^2 area UDT Sensors, Inc. silicon detector at constant illumination as a function of temperature at operating points between 130 and 324 mV.

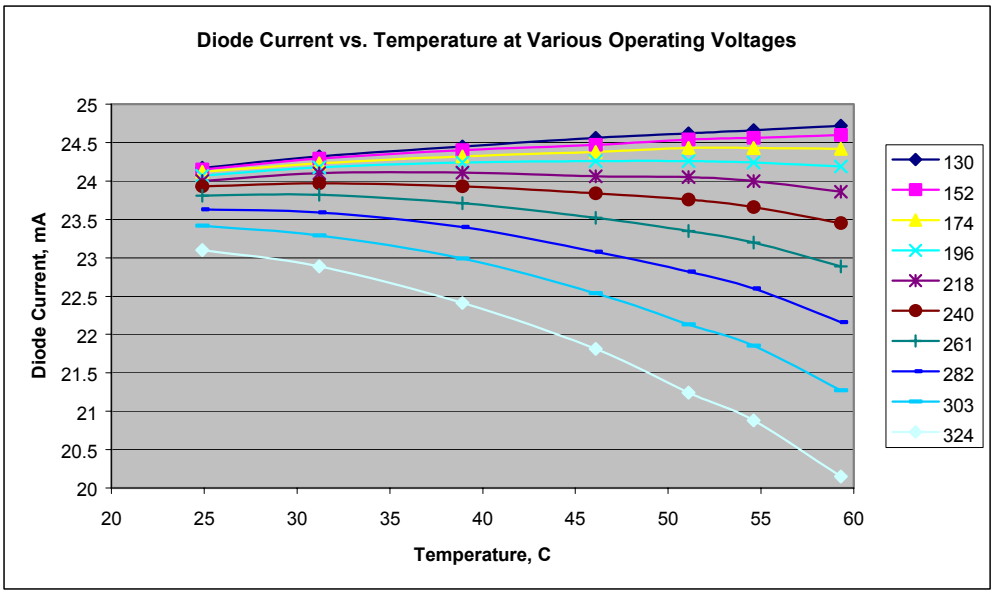

Figure 25: Effect of Temperature on Diode Current at Different Operating Points

Even though the changes are not linear, there is a significant, nearly straight region at the lower voltages, and at 223 mV, interpolated from the above data; the output is constant to within 0.35% over the 20 to 50° C temperature range. At short circuit, the output variation over this temperature range would be a factor of approximately five times higher, corresponding to a temperature coefficient of 0.11%/°C. Testing under somewhat different conditions, using a constant load on the diode to achieve an operating point, instead of fixing it directly, showed that the "zero" temperature coefficient point to vary slightly with intensity. Whether this is the case with a well-defined operating point is not known.

B. Comparing Indoor and Outdoor Jsc Measurements of Small Area Devices

Since ALS measurements results are relied on to provide rapid feedback on the effectiveness of process improvements, and because some of the results seemed to be incorrect, it was decided that it was necessary to characterize the accuracy of this system and compare it to outdoor test measurements. In this analysis, a series of small area devices (~0.18 cm^2) was tested on the ALS system and the on the quantum efficiency (QE) system, and compared to outdoor measurements.

Since significant spectral and intensity variations were expected between the three test systems, characterizing the Jsc was the focus of the tests for each of the 14 small area cells used in this analysis. The first test used the ALS system; this system employs an ELH lamp and a set of filters to roughly simulate the solar spectrum. The cells were then tested using the calibrated QE system, and then finally tested outdoors on a clear day at noon. The outdoor measurements were corrected for intensity using a small c-Si cell with a filter to make its response similar to a-Si. The Jsc measured using each of these systems was significantly different as shown in Table 15.

Table 15: Comparing Jsc Obtained with Different Light Sources

Measurement Method	Average Jsc (ma/cm^2)	% of Outdoor Jsc
ALS System	5.10	77%
QE System*	5.83	88%
Outdoors	6.60	100%

*The QE Jsc measurement shown here is average of the lower (limiting) Jsc in the tandem

The Jsc's measured on the ALS system were unexpectedly low compared to the outdoor measurements. Upon further investigation, it was observed that almost all tandem cells appeared to be front limited when tested on this system, even when the QE data indicated that they were either balanced or back limited. A plot of the front cell (Jsc1) versus the total current is seen to be very well correlated, as shown in Figure 26, which indicates that the front current is limiting the total current, when measured on the ALS. As shown on the graph this is true for cells that appear to be back limited (Jsc1/Jsc2 > 1) as well as for those that are front limited (Jsc1/Jsc2 < 1), as measured on the QE system.

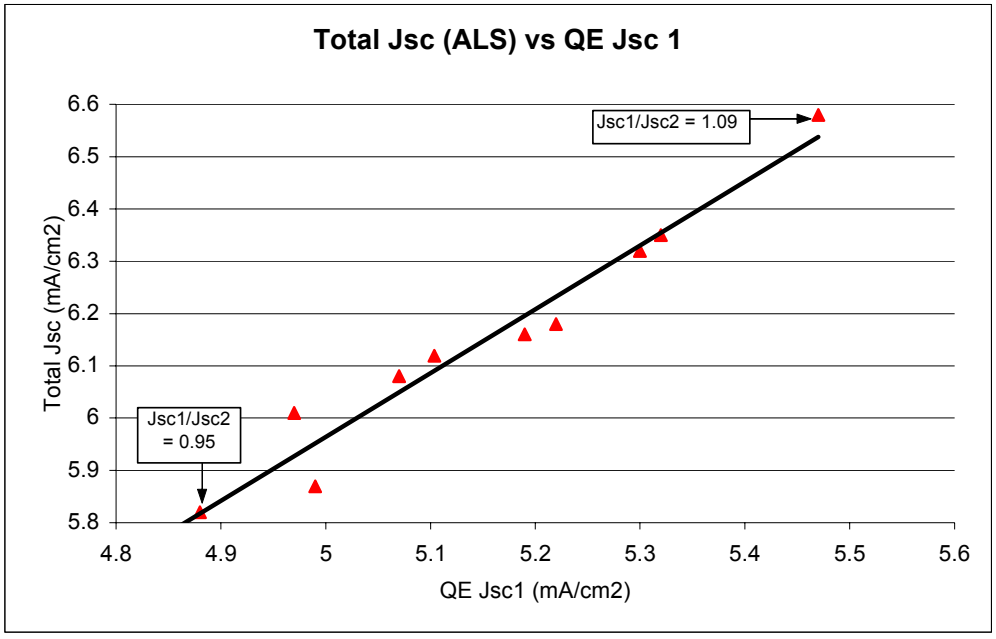

Figure 26: Comparison of Jsc1 from IV curve and from QE Determination

This contradiction between the ALS data and the QE data indicated that the ALS spectrum is not currently correct for standard tandems. Based on these data, it appears that the ALS light source is deficient in the blue portion of the spectrum, causing the cells to be front limited.

When the same cells are measured outdoors under near AM1.5 conditions, they have higher currents due to the increased blue light available. To correct this spectral problem, a new ELH lamp with more blue irradiance was installed into the ALS system and the cell current increased approximately 5% as they became less front limited. While this change did not completely fix the spectral problem of the light source, it was clearly a change in the right direction. Consequently, the system is being modified further to optimize the light source in order to more closely match the outdoor response of tandems cells outdoors.

The QE current also appears to be about 12% low based on the outdoor measurements. Since the QE system is calibrated before each test session from a known stable crystalline tandem Si-Ge cell, it is not obvious how this system may have drifted from its calibration, or if it did at all. This system is being examined and rechecked against the outdoor measurements more closely to identify potential sources of error. While past experience indicates that these systems are not completely equivalent, it is believed that the agreement between them can be improved.

C. Outdoor Light Soak and Indoor Accelerated Light Soak Comparison

It is commonly understood that there is no substitute for actual outdoor testing to evaluate the reliability of a PV product in the field. However, because the initial stabilization takes several months and then seasonal variations require an additional several months to reveal the long-term behavior of the modules, outdoor testing can take many months to complete. To obtain timely feedback on process changes, it is therefore necessary to develop accelerated indoor tests to speed the development process. The most common indoor reliability test for a-Si products is the accelerated light soak (ALS) test. This type of test can be performed on full sized modules, typically at one-sun intensity, or on small area devices at higher intensities, and it is a very useful tool to evaluate the effect of process changes on stability. Over the past several months, EPV has carried out a study to compare the results of ALS testing to the light induced degradation caused by outdoor exposure on various thicknesses of a-Si. The goal of this work is to determine EPV's ability to predict the performance of a module outdoors, and to improve upon the current accelerated test.

At EPV, the most useful ALS test is one that is performed on a small area device (dot) that is ~0.18 cm^2 under a tungsten halogen ELH lamp at approximately 47 suns intensity. The EPV process is based on the process developed by Tonon, Li, and Delahoy at APS, Inc [5]. The device is placed in a computer-controlled system with automated optics that alternate between the high intensity light soak and a filtered ELH lamp for periodic IV tests at prescribed intervals during the light soaking. The entire test takes about 8 minutes.

The advantage of the ALS test is that it is a very quick way to make a comparative evaluation of a module's stability. The final results of a sample under test are compared to the historical average ALS degradation and a determination of the relative stability can be readily made. The disadvantage of this test is that the ALS uses a very intense light source that is not the same spectrum or intensity of the sun. As a result, the degradation of a cell is often greater than the degradation achieved under outdoor light soak.

To improve the understanding of the ALS test, 18 tandem a-Si modules with a wide range of a-Si thickness were selected and the ALS test was performed on small areas in each. Sections of the same samples were placed outdoors on a 2 axis tracker and put outdoors during sunny

days. The outdoor samples were measured periodically and compared with the indoor ALS. The results of the outdoor light soaking are shown in Figure 27.

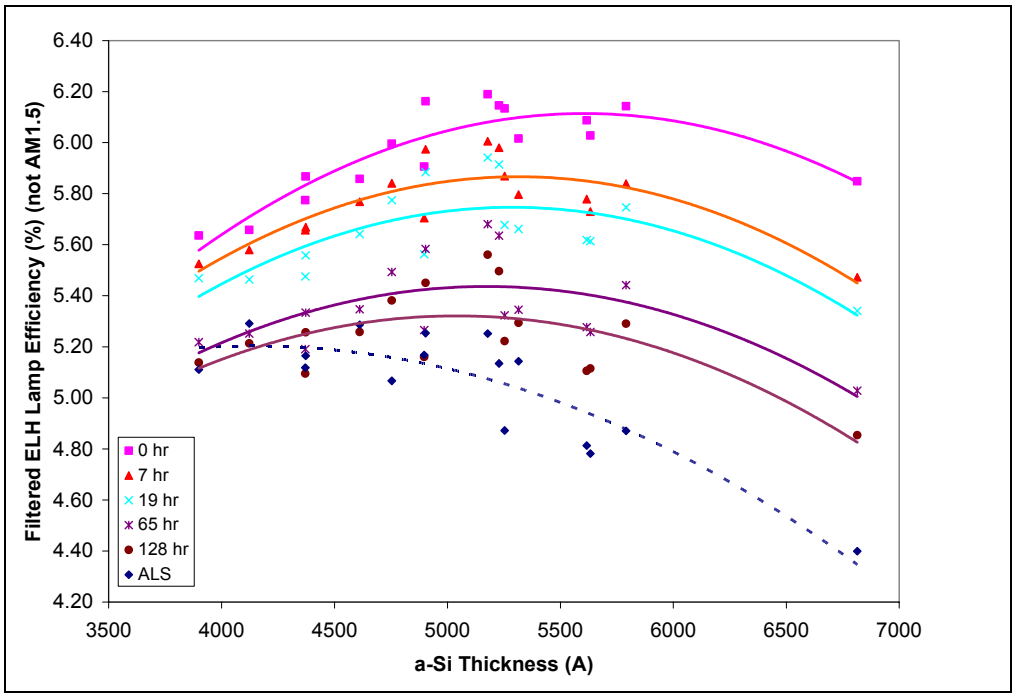

Figure 27: Relative Performance of Light Soaked Samples

The graph shows the typical loss in performance for the outdoor samples due to Staebler-Wronski degradation. As expected, the performance of the samples becomes progressively worse up to 128 hours of outdoor exposure to the sun. The dotted line indicates the performance of the companion samples after the indoor ALS. It is interesting to note that except for the thinnest samples, the ALS was more severe than the outdoor exposure.

Figure 28 shows the correlation of the ALS to the actual outdoor degradation at 128 hrs. The fit to the line is reasonably good and it seems to indicate that the ALS is a good predictor of outdoor light soak performance at 128 hrs, within perhaps ±3%. This agreement is a significant result, especially considering that such a rapid test such as the 8 minute ALS test is able to predict approximate 128 hr outdoor light soak results.

The samples were continued to be light soaked for a total of 544 hours outdoors and the performance did not change significantly from the 128-hour point for most devices. The samples have exhibited some seasonal variation during the hot summer months as the a-Si annealed and improved, and then began to decrease as the samples were continued to be light soaked into the autumn. These samples will be continued to be light soaked and monitored through the winter and the correlation will be expanded to more fully characterize their seasonal performance.

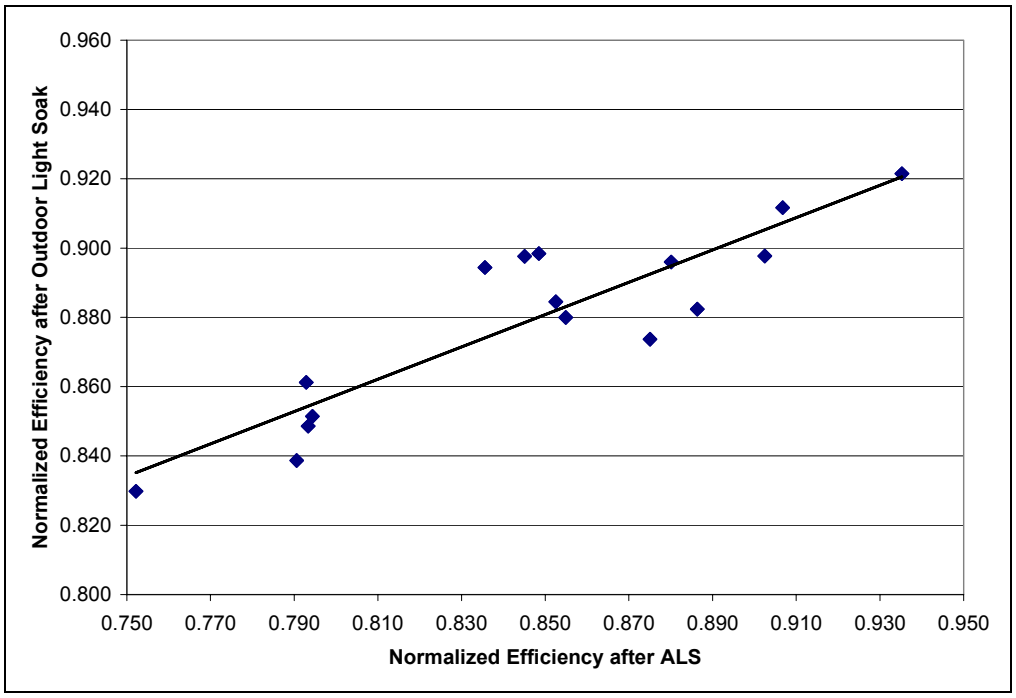

Figure 28: Normalized Efficiency of Tandem Samples after ALS vs. Outdoor Light Soak

D. LED Light Sources

To avoid the limitations of the incandescent lamp based IV tester light source and to add some flexibility to the measurements, an IV tester was assembled using several LED based light sources. Originally, the intention was to use a large number of different wavelength LEDs to approximately simulate AM1.5 conditions. From a geometric viewpoint this became difficult so the decision was made to represent only two or three regions of the spectrum and rely on the reproducibility of the a-Si films. From measurements made thus far, it appears that, with few exceptions, the major difference between different a-Si devices is the thickness ratio of the two stacks; the shape of the QE curves for most devices is reasonably constant. With that as a starting assumption, a light source based on LEDs can provide information on the relative current contribution of the two stacks and have enough intensity to make IV measurements meaningful.

One such LED based light source was constructed with three LEDs, red, green and blue, with center wavelengths of approximately 630, 520 and 460 nm, respectively.

As a first attempt at calibrating this light source, several IV curves were obtained for a very unbalanced device (Jsc1/Jsc2 ratio of 0.68). Figure 29 shows four of these, one in sunlight and the other three with the LED light source. For the LED measurements, the blue intensity was varied to first result in a good match to the sun IV curve, and then with too much and then too little blue. The latter two show the range of adjustment available.

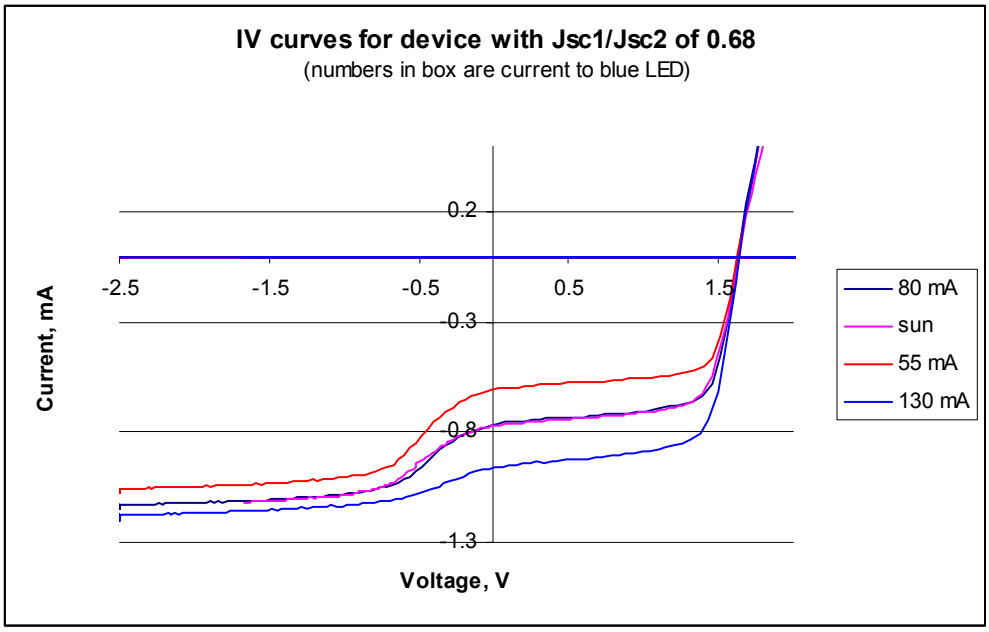

Figure 29: IV Curves in Sunlight and with LED Light Source

A second LED based light source was constructed using two high power LED's and a beam splitter so that the light beam from the two LED's appear to have the same origin, thus tending to make positioning of the dot less important. This source was compared to sunlight by measuring the Isc of several small cells as shown in Figure 30. The cells measured are from two experimental runs for which Jsc1/Jsc2 current rations vary from 0.78 to 1.49; two types of back reflectors are included in these data, Al only and Al/ZnO to evaluate the ability to correctly measure Jsc gains in the red end of the spectrum.

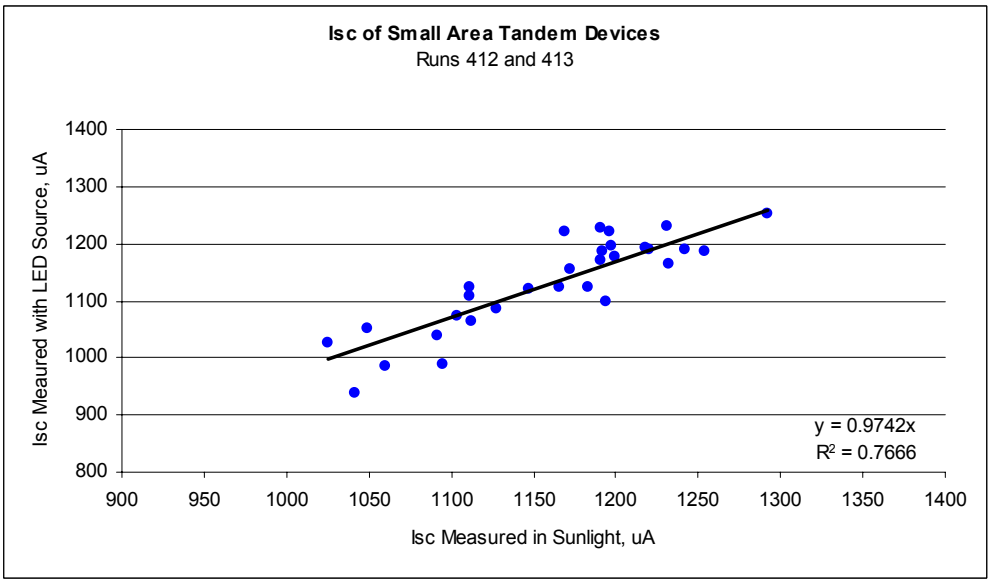

Figure 30: Comparison of Isc Obtained with an LED Based Light Source and in Sunlight

The correlation between the two sets of Isc's is reasonably good. It is a significant improvement over similar tests comparing outdoor tests to the ALS station Isc measurements, which showed poorer correlation, particularly with samples that used a ZnO/Al back reflector.

The improved correlation indicates that the spectrum of the LED light source is closer representation of AM1.5 than is the light source currently used at the ALS station.

References

[1] ASTM C158, Standard Test Methods for Strength of Glass by Flexure (Determination of Modulus of Rupture).

[2] 1. I. Muirhead and B. Hawkins, Annual Conf. Australian and New Zealand Solar Energy Society – SOLAR '96.

[3] Jansen, K.W. and Delahoy, A.E. "A Laboratory Technique for the Evaluation of Electrochemical Transparent Conductive Oxide Delamination from Glass Substrates", Thin Solid Films vol. 423/2, 2003, pp 153 - 160.

[4] Kothandaraman, C., Tonon, T., Huang, C., Delahoy, A.E., "Improvement of a-Si:H P-I-N Devices using Zinc Oxide Based Back-Reflectors", Mat. Res. Soc. Proc., Vol. 219, 1991, pp. 475-480.

[5] T. Tonon, X. Li, A.E. Delahoy, "Accelerated Light Soaking and Prediction of One-Sun Photostability in a-Si:H Solar Cells", 21st IEEE Photovoltaic Specialists Conf. Orlando, May 1990.

REPORT DOCUMENTATION PAGE

Form Approved
OMB No. 0704-0188

PLEASE DO NOT RETURN YOUR FORM TO THE ABOVE ORGANIZATION.

1. REPORT DATE *(DD-MM-YYYY)*	2. REPORT TYPE	3. DATES COVERED *(From - To)*
February 2005	Subcontract Report	October 2001–December 2004

4. TITLE AND SUBTITLE
Productivity Enhancement for Manufacturing of Amorphous Silicon PV Modules: Final Technical Progress Report, 1 July 2002–31 October 2004

5a. CONTRACT NUMBER
DE-AC36-99-GO10337

5b. GRANT NUMBER

5c. PROGRAM ELEMENT NUMBER

6. AUTHOR(S)
H. Volltrauer and K. Jansen

5d. PROJECT NUMBER
NREL/SR-520-37659

5e. TASK NUMBER
PVB56101

5f. WORK UNIT NUMBER

7. PERFORMING ORGANIZATION NAME(S) AND ADDRESS(ES)
Energy Photovoltaics, Inc.
276 Bakers Basin Road
Lawrenceville, New Jersey 08648

8. PERFORMING ORGANIZATION REPORT NUMBER
ZDO-2-30628-14

9. SPONSORING/MONITORING AGENCY NAME(S) AND ADDRESS(ES)
National Renewable Energy Laboratory
1617 Cole Blvd.
Golden, CO 80401-3393

10. SPONSOR/MONITOR'S ACRONYM(S)
NREL

11. SPONSORING/MONITORING AGENCY REPORT NUMBER
NREL/SR-520-37659

12. DISTRIBUTION AVAILABILITY STATEMENT
National Technical Information Service
U.S. Department of Commerce
5285 Port Royal Road
Springfield, VA 22161

13. SUPPLEMENTARY NOTES
NREL Technical Monitor: R. Mitchell

14. ABSTRACT *(Maximum 200 Words)*

The overall objective of this subcontract over its two-year duration is to continue the advancement of Energy Photovoltaics, Inc.'s (EPV) a-Si production manufacturing technology and improve the production equipment used in manufacturing. This will allow EPV to reduce module costs by increasing module output, throughput, and yield. EPV conducted parallel research efforts for achieving higher stabilized module power output through improvements in several manufacturing processing steps, with particular emphasis on the thin-film deposition process. The dual goals of achieving a 20% gain in stabilized output and a 20% reduction in direct costs were accomplished. The 20% gain in stabilized output increased the power of the standard 0.79 m^2 module to about 45 watts. This was achieved through optimizing the a-Si deposition process to improve stability, increasing the active area of the module, and developing a ZnO/Al back reflector to increase the light absorption of the a-Si. Additionally, improvements were made to the a-Si uniformity, and an improved TCO was incorporated into the standard product. The goal of reducing costs by 20% was exceeded, resulting in an estimated direct cost of $1.41/W, for the process in EPV's New Jersey facility. This was accomplished through a complete review of the process that resulted in lower material costs, lower labor costs, less downtime, and higher module power, as noted above. The process was streamlined and made more efficient by eliminating or combining process steps, and selected processes were automated. In addition, improvements were made to the characterization and measurement techniques used in the module optimization process.

15. SUBJECT TERMS
PV; module; solar cells; manufacturer; production equipment; output and throughput; thin-film; back reflector; light absorption; characterization and measurement; optimization process

16. SECURITY CLASSIFICATION OF:			17. LIMITATION OF ABSTRACT	18. NUMBER OF PAGES	19a. NAME OF RESPONSIBLE PERSON
a. REPORT	b. ABSTRACT	c. THIS PAGE			
Unclassified	Unclassified	Unclassified	UL		19b. TELEPONE NUMBER (*Include area code*)

Standard Form 298 (Rev. 8/98)
Prescribed by ANSI Std. Z39.18